Recent Advances in the 18-electron Complex Transition Metal Hydrides of Ni, Fe, Co and Ru

Terry D. Humphries [a]*, Drew A. Sheppard[a] and Craig E. Buckley[a]

[a] Department of Physics and Astronomy, Fuels and Energy Technology Institute, Curtin University, GPO Box U1987, Perth, WA 6845, Australia.

* terry_humphries81@hotmail.com

Abstract

Metal hydrides have received much attention due to the flourishing concept of a hydrogen economy. In addition, recent studies of metal hydride materials have shown that technological implementation of these compounds not only lies in the storage of hydrogen, but for a range of multi-functional applications; including, smart optical windows, energy storage materials in fuel cells for both stationary and mobile devices, and as thermal energy storage materials for concentrating solar thermal plants. This review concentrates on the molecular structures, thermodynamic properties and other physical properties of the complexes of $[NiH_4]^{4-}$, $[FeH_6]^{4-}$, $[CoH_5]^{4-}$ and $[RuH_6]^{4-}$. The synthesized derivatives of these compounds have also been reviewed to give a full overview on the advancement of these systems and will allow for a fresh prospective for future studies to fully understand the physical and chemical nature of these complex transition metal hydrides.

Keywords: Complex transition metal hydride; thermodynamics; structure; hydrogen storage; thermal energy storage; review.

Contents:

1. Introduction

Complex metal hydrides have found prominence as hydrogen storage materials in recent years due to their hydrogen capacity and purity of desorbed hydrogen. For instance, Mg_2FeH_6 has the capacity to release 5.6 wt.% of pure hydrogen [1], unlike its $Mg(BH_4)_2$ equivalent, which releases toxic B_2H_6 as an impurity [2]. Another advantage to complex transition metal hydrides is that they can be reformed after hydrogen desorption, by the direct reaction with hydrogen gas, fundamentally making them ideal candidates for energy storage applications.

In the simplest compositions of these systems, all hydrogen atoms are bonded to the transition metal center T giving the chemical formula $M_m{}^{\delta+}[TH_n]^{\delta-}$ (T = 3d, 4d, 5d elements; M = alkali, alkali-earth and rare-earth elements; m, n = 1, 2, 3 ….) [3]. The transition metals contained in these homolyptic mononuclear hydride complexes range from Group 7 to Group 12, although for hydrogen storage research purposes 3d elements retain the majority of the focus. That being said, hydride complexes of the 4d and 5d transition metals have been synthesized, excluding Ag, Au and Hg.

Complex transition metal hydrides can adopt a variety of electronic configurations and ligand geometries including linear, tetrahedral to tricapped trigonal prismatic [4, 5]. This structural assortment is due to the ability of transition metal hydrides to possess a variety of oxidation states combined with the flexible nature of the hydride ligand, which can be found to bond as a covalent ligand or anion within the same structure. The small atomic size and high-field ligand character of hydrogen leads to the preferential formation of 18-electron complexes, although 16 or 14 electron complexes have been reported for Rh, Pt, and Pd. This electronic flexibility afforded by the transition metals, with incorporation of additional cations leads to an abundance of complexes to be formed.

The hydrogen capacity of the complex hydrides tends to decrease as the number of available bonding electrons from T increases. The 18-electron hydride complexes of octahedral $[FeH_6]^{4-}$, square-pyramidal $[CoH_5]^{4-}$, and tetrahedral $[NiH_4]^{4-}$ exemplify this situation effectively, with T having $d6$, $d7$ and $d8$ electronic configurations, respectively (Fig. 1). Accordingly, the hydrogen capacity of these complexes decreases and as consequence the high capacity Mg_2FeH_6 compound has been subject to greater scrutiny than the Ni and Co analogues. The plethora of articles published since the turn of the century on the complexes of $[NiH_4]^{4-}$, $[FeH_6]^{4-}$, $[CoH_5]^{4-}$ and $[RuH_6]^{4-}$, as well as those dating back from the 1960's, has prompted a requirement for a literary review to collate the information that has been meticulously measured and calculated by various methodologies. Several of these articles describe the synthesis and characterization of polymorphs and analogues of the archetypal $Mg_2[TH_n]^{\delta-}$ (T = Ni, Fe, Co, Ru) complexes [6-17]. In addition, vibrational spectra of these hydrides have been recently reviewed [18].

(Fig. 1)

More recently, transition metal complexes stabilized by quasi-isolated H$^-$ have also been introduced, which increases the total anionic charge of the system, thus allowing for a greater variety of cation coordination and hence the number of compounds able to be formed [19-28]. This recent expansion of the number of complexes and the breadth of analyses being undertaken on each has shown that technological application of these compounds not only lies in the storage of hydrogen, but also possibly for a range of multi-functional applications, including solid state batteries, smart windows, thermal energy storage materials and magnetic refrigeration [29-34]. In particularly, the relatively high thermodynamic stability of complex transition metal hydrides has provided recent interest in metal hydrides for high temperature heat storage applications [31-33] and neutron moderators or nuclear fuel components in nuclear reactors [35].

This review concentrates on the molecular structures, thermodynamic properties and other physical properties of the complexes of $[NiH_4]^{4-}$, $[FeH_6]^{4-}$, $[CoH_5]^{4-}$ and $[RuH_6]^{4-}$. The discussion order starts with the most well-characterised complex, $[NiH_4]^{4-}$, and finishes with the least characterized complex, $[RuH_6]^{4-}$. The synthesized derivatives of these compounds have also been reviewed to give a full overview on the advancement of these systems and will allow for a fresh prospective for future studies to fully understand the physical and chemical nature of these complex transition metal hydrides.

2. Complexes of $[NiH_4]^{4-}$

2.1. Mg$_2$NiH$_4$

The synthesis and characterization of Mg$_2$NiH$_4$ was first reported in 1968, along with the realization that the compound could feasibly be employed as a hydrogen storage material [13]. The synthesis of Mg$_2$NiH$_4$ involves a simple sintering of the Mg$_2$Ni alloy, under 30 bar H$_2$ at 200 °C (Eq. 1). In the initial report by Reilly and Wiswall, it was identified that the brick red product undergoes reversible hydrogenation at 325 °C and 21 bar of H$_2$ pressure with $\Delta H_{des} = -64.4$ kJ/mol H$_2$, and a theoretical hydrogen capacity of 3.62 wt% H$_2$ [13].

$$\text{Mg}_2\text{Ni} \quad \xrightarrow{\text{200 °C, 30 bar H}_2} \quad \text{Mg}_2\text{NiH}_4 \quad (1)$$
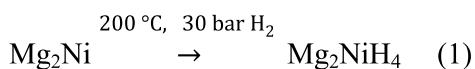
Since the discovery of Mg$_2$NiH$_4$, many articles have been published concerning molecular structure, physical properties and hydrogen storage applications [34, 36-45]. At first glance, this molecule appears to comprise of simple $[NiH_4]^{4-}$ tetrahedra stabilized by Mg^{2+}, (Fig. 2a, b). On the contrary, the structure of Mg$_2$NiH$_4$ is quite intricate and, as a result, has allowed for a rich debate. Early thermodynamic and calorimetric studies of this compound have led to the discovery of two low temperature and two high temperature phase modifications, of which have been investigated in depth and could possibly be subject to a review in their own right. Unfortunately, this article will only traverse the structural and thermodynamic aspects of these phases, although the references contained within will allow for a more in depth study.

(Fig. 2)

The LT to HT phase transition was first identified, and subsequently crystallographically characterized, to occur between 210 − 245 °C in 1979 [46]. The authors originally identified the low temperature phase to crystallize in the orthorhombic space group, while the HT phase was identified to crystallize in a cubic pseudo-CaF_2-type structure with a = 6.490 Å (Fig. 2c,d). Additionally, the enthalpy associated with the phase change was determined to be 6.69 kJ/mol Mg_2NiH_4. Unfortunately, the original data of the LT phase was misconstrued and the actual structure was in debate for several years, with various models being presented from both neutron and X-ray diffraction data [38, 47-51]. Noréus and Werner suggested an octahedron model, in which four hydrogen atoms form a square plane centered on a nickel atom [47]. Meanwhile, Zolliker et al. proposed a tetrahedral model, where four hydrogen atoms occupy the four corners of the tetrahedron centered on a nickel atom [38]. Fortunately, with the aid of NMR spectroscopy [37], quantum chemical calculations [48] and *ab initio* calculations [39, 44], the model has been determined to be a tetrahedrally distorted square-planar configuration of hydrides around the nickel metal center forming $[NiH_4]^{4-}$ (Fig. 2a). The $[NiH_4]^{4-}$ unit is close to a regular tetrahedron, with Ni–H bond lengths ranging from 1.519 to 1.572 Å (average 1.54 Å) and H–Ni–H bond angles averaging 109.4° (Table 1) [52]. The eight $[NiH_4]^{4-}$ moieties in each monoclinic unit cell (Space group *C2/c*) are crystallographically equivalent, but have four different orientations with respect to the crystal axes. The structure exhibits a slightly monoclinically distorted antifluorite structure, with the $[NiH_4]^{4-}$ complex being surrounded by a distorted cube of magnesium ions (Fig. 2b) [36, 46].

The structural variation between the LT and HT phases are small but have been studied in depth. Even to date, the H position of the HT phase have not been fully elucidated by diffraction methods. It has been ascertained by neutron diffraction that the Mg and the $[NiH_4]^{4-}$ are arranged in a regular antifluorite structure, with the hydrides rotating in a 1.5 Å sphere around the Ni center (Fig. 2d) [53]. DFT calculations by Garcia et al. using a local density approximation (LDA) [44], also concluded that H surrounded the Ni in a distorted tetrahedron, with Ni−H distances of 1.548 Å (Fig. 2c). Subsequent First Principles calculations on the HT phase are also in good agreement with the results reported by Garcia et al.

(Table 1)

While investigating the true structure of the LT phase, and in particular identifying the reason for the disparity between obtained unit cells, it was realized that the phase change influenced the crystallinity of the LT phase. More precisely, the method of synthesizing the LT phase affects the long-range crystallization of the material. The phase transition was observed to be reversible, although upon cooling from the HT phase, stacking-faults are introduced causing microtwinning on the unit-cell level [54, 55]. This microtwinning can be suppressed leading to two modifications of the LT phase, LT1 with and LT2 without microtwinning. Suppression is achieved by synthesizing Mg_2NiH_4 below 235 °C, ultimately inhibiting the rotation of the H atoms around the Ni metal center. The difference between the two modifications is the appearance of extra peaks in the XRD pattern due to the microtwinning. These peaks are thus responsible for the complications in indexing the LT phase [54]. A detailed summary concerning the microtwinning of the LT phase is contained within reference [36].

Generally, the phase transition of the HT to LT modification occurs at 237 °C and a number of experiments have been conducted to investigate the true behavior of this solid-state phase change. A twin-cell heat conduction (Tin-Covets) calorimetric study by Post and Murray was conducted in 1987, after synthesizing Mg_2NiH_4 at temperatures above and below the phase transition temperature and scanning the materials slowly over the temperature range of the phase transition [56]. The authors noted the existence of three LT and two HT structural modifications between 117 and 327 °C, within the pressure range of 6 to 40 bar. One modification, LT3, showed thermal characteristics attributable to gross structural and/or compositional inhomogeneity. The remaining four modifications exist in two reversible pairs, LT1 + HT1 and LT2 + HT2, the enthalpies of transition for which are ΔH_{tr} = 3.99 ± 0.05 kJ/mol H_2 and 4.16 ± 0.04 kJ/mol H_2, respectively. Using *ab initio* total-energy density functional theory, Myers et al. calculated the ΔH of the phase transition to be 0.325 ± 0.03 eV per f.u. [39]. The authors noted that previous determinations from calculations may not have used a HT model with the lowest energy structure and that expanding the unit cell may allow the $[NiH_4]^{4-}$ units to assume different spatial orientations. The model previously used assumed that all $[NiH_4]^{4-}$ units have identical orientations [44], whereas neutron scattering experiments indicated that the H atoms fluctuate around the central Ni atom [53].

Mg_2NiH_4 is an 18-electron complex and as such should be an insulator, although measurements have shown that the LT phase is in fact a semi-conductor [30, 39, 43]. The easily polarizable hydride ions help to distribute the high electron density of the d^8 central transition-metal by outward bonding to the surrounding counterions, which leads to electric conductivity. One major effect of the introduction of microtwinning into the Mg_2NiH_4 lattice is that the ability to conduct is removed. This property may not be thermally reversed, although it has been reported that compaction of LT2 phase into tablets reduces the amount of twinning and conductivity is possible [36]. Myers et al. studied the thermodynamic, electronic, and optical properties of the LT phase by *ab initio* total-energy density functional theory [39]. Due to the high computational requirement to relax a system with 56 atoms and 20 independent degrees of freedom, this was the first investigation of the LT phase by DFT. The obtained optimized structure agreed very well with that obtained from neutron diffraction with a maximum atomic position difference of 0.14 Å [38]. The electronic structure of LT Mg_2NiH_4 calculated by Myers et al. resembles that of cubic Mg_2NiH_4 with an undistorted tetrahedral hydrogen configuration [39]. This result corroborates those previously calculated by Garcia et al [44]. In both cases, there are four low-lying bands per formula unit. These are H states and are separated by a gap from another five occupied bands, the Ni $3d$ bands. The calculations suggest that both phases are indirect semiconductors with the LT phase having an indirect band gap of 1.4 eV. This value agrees with the value calculated by Häussermann et al. of 1.54 eV [43] and the experimental value of 1.68 eV [30]. The lower symmetry of LT Mg_2NiH_4, compared to the HT phase, produces a shoulder in its dielectric constant that does not appear in the HT phase. This reduces the optical gap by approximately 0.5 eV compared to that of the HT Mg_2NiH_4 phase [39].

Due to the ease of synthesis and simple structure, a number of studies into the physical properties of $MgNiH_4$ and its deuterium analogue have been conducted. ^{1}H and ^{2}H solid-state NMR spectroscopy studies were carried out on the low temperature phase over the temperature range of −73 to 67 °C and the observed line shaped simulated [37]. Overall, this study detected a temperature

dependence arising from the distorted tetrahedral configuration and a pseudo-isotropic rotation of the $[NiD_4]^{4-}$ unit. The ^1H NMR spectroscopy measurements indicate that the second moments are 202 kHz^2 in the rigid lattice (supporting the tetrahedral coordination) and 46.6 kHz^2 in a motional state (isotropic rotation of the $[NiD_4]^{4-}$ unit). Below -13 °C, the ^2H spins are in a rigid state and can be deconvoluted into four peaks, attributed to at least four crystallographically independent sites. ^2H NMR spectroscopy data determined Mg_2NiD_4 to possess a jump frequency factor of $0.8 \pm 0.6 \times 10^{13}$ Hz and activation energy of 50.1 ± 1.4 kJ/mol. At the same time, neutron diffraction experiments also conclude that in the high temperature phase, the jumps of the H atom occur in spherical symmetry on the octahedron and most likely that four H atoms form a square planar unit, which randomly flip around the Ni atom [53]. The low temperature phase of Mg_2NiH_4 was also studied indicating no other mobility of the hydrogen atoms other than a vibrational motion.

The infrared, Raman and ineleastic neutron scattering (INS) spectra of Mg_2NiH_4 have also been collected while INS was also carried out on Mg_2NiD_4 [57]. Mg_2NiH_4 was modelled with T_d symmetry allowing normal selection rules to be applied despite the observed distortion in the molecule. Assignment of the spectra determined that the stretching mode occurs at 1691 cm^{-1} (A_1) in the Raman and INS spectra and 1674 cm^{-1} in the infrared spectrum (T_2). Additionally, the structure and dynamics of hydrogen in Mg_2NiH_4 has been studied by elastic and inelastic neutron scattering [53].

The reversible hydrogenation of Mg_2NiH_4 thin films yields an electrochromic mirror electrode, or switchable mirror [58]. These Smart Optical Windows (SOW's) employing Ni are environmentally and financially effective compared to the rare earth-magnesium alloy counterparts [59], which are easily oxidized and incur phase separation [60]. The dehydrogenated Mg-Ni alloy is a mirror when layered as a thin film, while passing a dry gas stream of 4 % H_2 in Ar or He hydrogenates the alloy forming a transparent film on the glass substrate. The mirror state can be recovered by exposing the films to ambient air. Covering the films with a Pd overlayer enhances the gasochromic transition rate of the film and increases the overall transition yield, while protecting the metals from oxidation. An optimal transition speed of 10 s was achieved by a gasochromic reaction, which was four times faster than that achieved using electrochemical reactions. Switching to the clear state was achieved in 40 s and to the mirror state in 90 s by stepping the potential to -1.2 and -0.2 V, respectively. Since the time of this innovative discovery, an assortment of articles have been published concerning thin film Ni-Mg alloys for SOW and hydrogen storage applications. These studies include methods of thin film production, microstructure analysis, Pressure-Composition-Temperature (PCT) measurements, *in situ* X-ray absorption spectroscopy, elipsometric studies and determination of their optical properties [29, 61-68].

2.2. Mg_2NiH_4 Analogues

To date, only seven $[NiH_4]^{4-}$ complexes have been crystallographically characterized; Mg_2NiH_4, $Na_2Mg_2NiH_6$, $EuMgNiH_4$, $CaMgNiH_4$, $SrMgNiH_4$, $YbMgNiH_4$ and $LaMg_2NiH_7$ (Fig. 3, Table 1) [27, 38, 69-72]. A pseudo-$[NiH_4]^{4-}$ complex, $La_2MgNi_2H_8$, has also been reported [19]. It is apparent that tetrahedral $[NiH_4]^{4-}$ is observed to primarily form complexes containing Mg^{2+} and it

seems that the strongly polarizing Mg^{2+} counterion is required to stabilize the relatively weak $[NiH_4]^{4-}$ complex [73].

(Fig. 3)

$EuMgNiH_4$, $CaMgNiD_4$, $SrMgNiD_4$ and $YbMgNiD_4$ crystallize in the cubic $P2_13$ space group with each $[NiH_4]^{4-}$ tetrahedron being surrounded by a deformed cube of alkaline earth atoms (Fig. 3a) [70, 71]. The average Ni−D bond lengths in these complexes are longer than the corresponding Ni−D bond lengths in Mg_2NiD_4 with the metal-deuterium bond lengths increasing in the order of Mg < Ca < Yb < Sr (1.53(2), 1.601(8), 1.608(7), 1.614(8) Å respectively, Table 1) [38, 70, 71]. In addition, there is an inherent increase in unit cell parameters with Yb < Ca < Sr (6.7114(6), 6.7301(4), 6.8953(4) Å respectively) which is expected with matrix effects. As with Mg_2NiH_4, the cubes are edge-sharing with the $[NiD_4]^{4-}$ tetrahedron being separated by empty alkaline-earth cubes. The resulting metal atom arrangements can be described in terms of a deformed CaF_2 type structure.

The structures of $LaMg_2NiH_7$ and $Na_2Mg_2NiH_6$ are also of interest, as unlike the MMgNiH$_4$ (M = Sr, Eu, Yb, Ca, Mg) analogues, these compounds display both ionic and covalently bonded hydrides and are seen as a link between 'interstitial' and 'complex' metal hydrides. In $LaMg_2NiH_7$ ($La^{3+}\cdot2Mg^{2+}\cdot3H^{-}\cdot[NiH_4]^{4-}$), the $[NiH_4]^{4-}$ complex is surrounded by a mono-capped square anti-prism of nine cations (six Mg^{2+} and three La^{3+}) (Fig. 3b) [72]. The ionic hydrides (H$^-$) are bound to La and Mg only in tetrahedral [La_2Mg_2] moieties, reminiscent to those of saline hydrides. Resistivity measurements and DFT calculations confirm the structural model and also the metallic to semi-conductor transition during hydrogenation [74].

The recent characterization of the quaternary complex $Na_2Mg_2NiH_6$ ($2Na^+\cdot2Mg^{2+}\cdot2H^-\cdot[NiH_4]^{4-}$) highlighted the first identification of an alkali metal directly stabilizing a $[NiH_4]^{4-}$ complex [27, 69]. In this compound, the $[NiH_4]^{4-}$ is surrounded by two Na^+ and two Mg^{2+} ions (Fig. 3c), while the ionic hydrides are coordinated four-fold by $2Mg^{2+}$ and $2Na^+$ ions [69]. The average Ni−D distance in this compound is 1.61(2) Å which is significantly longer than that of Mg_2NiH_4 indicating the mutual contribution of both countercations on the $[NiD_4]^{4-}$.

The enthalpy of desorption of the $[NiH_4]^{4-}$ complexes vary considerably, with Mg_2NiH_4 having ΔH_{des} = 64.4 kJ/mol H_2, while $CaMgNiH_4$ has a ΔH_{des} = 129 kJ/mol H_2 [13, 70]. These values are not directly related to the electronegativity of the M atom, instead it appears that the thermal stability is governed considerably by the ΔH_f of the corresponding binary hydride (Table 1) [71]. To illustrate this point, ΔH_f of MgH_2 is −74.5 kJ/mol H_2 compared to −174.5 kJ/mol H_2 for $CaMgNiH_4$ [75]. This suggests that the M−H bonds (M = Ca, Mg, La, Na, Yb, Sr) in the structure contribute more to the thermal stability of the compound than the Mg−H or the Ni−H bond.

To date, the analysis of mixed metal $[NiH_4]^{4-}$ compounds is limited to crystallographic and thermodynamic data, although a recent first-principle DFT and DFT + U (density functional theory plus on-site coulomb interaction calculations) study of the Yb, Ca and Sr analogues of Mg_2NiH_4 has furthered the characterizations of these compounds [76]. The outcome suggests that the atomic radii of M effects the Ni−H distances as well as compressibility and structural stability. From Total Density of States (DOS) studies, the authors suggest that these materials are semiconductors and calculate the degree of molecular

interactions between the atoms in the crystal lattice. It is suggested that there are ionic interactions between M atoms and $[NiH_4]^{4-}$ units, strong covalent Ni–H interactions within the NiH_4 tetrahedral structure, and weak covalent interactions between Mg and H and M and H atoms. Lastly, from Bader charges, the authors suggest that the degrees of ionization of Ca, Sr and Yb atoms decreases in the following order: Ca > Sr > Yb.

Of the $[NiH_4]^{4-}$ complexes, $LaMg_2NiH_7$ has received much attention due to the reversible hydrogen storage properties, with calculated efficiencies of 2.8 wt% and 109.5 g/L [72]. The crystal structure was first reported in 2003 and subsequent hydrogen storage related studies have since been pursued [74]. The hydrogen free $LaMg_2Ni$ alloy absorbs hydrogen at less than 200 °C and 8 bar H_2 pressure, changing from a metallic compound with an orthorhombic structure (space group $Cmcm$) to the hydride with monoclinic symmetry (space group $P2_1/c$). This structural change is only slight, with a shift of all atoms being less than 0.7 Å. DSC experiments confirm that H_2 absorption (initial H_2 pressure of 0.24 bar) occurs above 170 °C, but when heated above 250 °C disproportionation occurs, leading to the formation of the stable La-hydride and Mg_2Ni alloy [77]. The ΔH_{abs} was determined to be −94 kJ/mol H_2 by PCI measurements inside a volume calibrated DSC at 170 °C. Further absorption experiments have determined that uptake of hydrogen occurs at 30 °C under 1 bar H_2 pressure, forming $LaMg_2NiH_x$ ($x \simeq 5$), while at 200 °C $x \gtrsim 6.7$ [78]. An intermediate phase of $x = 4.6$ was determined by powder neutron diffraction with a space group $P2_1/m$. In this structure, clusters of $NiH_{1.9}$ and $NiH_{3.3}$ with fractional occupancies. DFT calculations identify that the $LaMg_2NiH_{4.6}$ phase has a ΔH_f of −88 kJ/mol H_2. This is only 5 kJ/mol H_2 lower than that calculated for $LaMg_2NiH_7$, which may explain why this intermediate phase has not been previously identified.
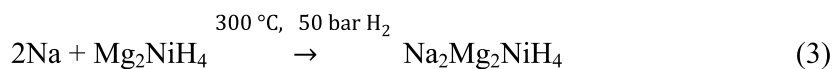
$La_2MgNi_2H_8$ is a dinuclear hydride consisting of isolated $[Ni_2H_7]^{7-}$ and $[Ni_4H_{12}]^{12-}$ complexes. The hydride and its deuteride analogue were synthesized by annealing La_2MgNi_2 under 30 bar $H(D)_2$ at 100 °C for 24 h [19]. The resultant powder has been analyzed by powder neutron and synchrotron diffraction, and its electrical resistance and magnetism studied. $La_2MgNi_2H_8$ crystalizes in the space group $P2_1/C$ with all Ni atoms surrounded by terminal and bridging deuteride ligands in an approximately tetrahedral configuration. The $[Ni_2H_7]^{7-}$ complex anion consists of a pair of Ni-centered tetrahedra, which share a corner deuterium, while the tetranuclear $[Ni_4H_{12}]^{12-}$ complex consists of four Ni-centered tetrahedra which each share two corners. The average terminal Ni−D bond distance is 1.58 Å, while the bridging Ni−D bond distance is an average of 1.61 Å. These distances are highly comparable to that of $Na_2Mg_2NiD_6$ (1.61(2) Å) [69], $LaMg_2NiD_7$ (1.59(2) Å)[72] and $SrMgNiD_4$ (1.614(8) Å) [71]. The three remaining deuterium atoms are bound as D^- to La_4Mg_2 or La_2Mg_2 moieties. Therefore, the limiting ionic formula of this compound is $8La^{3+}·4Mg^{2+}·[Ni_2H_7]^{7-}·2[Ni_4H_{12}]^{12-}·6H^-$. The $[Ni_2H_7]^{7-}$ and $[Ni_4H_{12}]^{12-}$ complexes can be regarded as an 18-electron complexes in that the Ni to terminal hydrogen bonds can be described as two-center two-electron bonds (2c-2e) while the bridging bonds are three-center two electron bonds (3c-2e).

Unfortunately, $La_2MgNi_2H_8$ does not desorb hydrogen reversibly owing to partial segregation into the binary hydride (LaH_3) and a secondary phase [19]. Therefore, the chances of this material finding technological application are low. The electrical resistivity of the La_2MgNi_2 precursor material is low, consistent with metallic behavior, while the hydride is semi-conducting, although unfortunately, the band-gap has not been determined. Magnetic measurements reveal that $La_2MgNi_2H_8$ is slightly ferromagnetic.

Recent ventures to synthesize novel rare-earth complex transition metal hydrides have allowed reports of REMg$_2$$T$ (RE = La, Pr, Nd, Ce; T = Ni, Pd, Pt) alloys which crystallize in the space group *Cmcm*, analogous to LaMg$_2$Ni [79, 80]. Unfortunately, during the hydriding of the Ni containing alloys at 30 bar H$_2$ at 350 °C, segregation was observed into RE−H and Mg$_2$NiH$_4$ [80].

2.3. Synthesis of [NiH$_4$]$^{4-}$ complexes

The synthesis of Mg$_2$NiH$_4$ is a simple hydrogenation of Mg$_2$Ni alloy, which requires the sintering of Mg$_2$Ni under 30 bar H$_2$ at 200 °C (Eq. 1) [13]. The synthesis of the M_xMg$_y$H$_z$NiH$_4$ complexes is achieved via three general routes, one method is alloying of the elements in stoichiometric ratios followed by reaction at temperatures above 450 °C under ~130 bar H$_2$ (Eq. 2) [70]. The second method is the sintering of a metal hydride with MgNiH$_4$ at 300 °C, under 50 bar H$_2$ (Eq. 3) [69]. The synthesis of LaMg$_2$NiH$_7$ required less harsh conditions, with the reaction of metallic La with Mg$_2$Ni at 200 °C and 8 bar H$_2$ being required (Eq. 4) [72]. Reactive milling of La$_{20}$Mg$_{50}$Ni$_{30}$ and La$_{25}$Mg$_{50}$Ni$_{25}$ under 5 bar H$_2$ pressure also results in the formation of nanostructured LaMg$_2$NiH$_7$ [81].

$$M + \text{Mg} + \text{Ni} \xrightarrow{450\ °C,\ 130\ \text{bar H}_2} M\text{MgNiH}_4 \ (M = \text{Sr, Eu, Yb, Ca}) \quad (2)$$

$$2\text{Na} + \text{Mg}_2\text{NiH}_4 \xrightarrow{300\ °C,\ 50\ \text{bar H}_2} \text{Na}_2\text{Mg}_2\text{NiH}_4 \quad (3)$$

$$\text{La} + \text{Mg}_2\text{Ni} \xrightarrow{200\ °C,\ 8\ \text{bar H}_2} \text{LaMg}_2\text{NiH}_7 \quad (4)$$

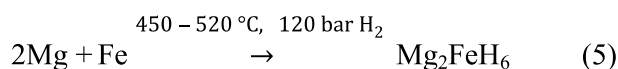## 3. Complexes of [FeH$_6$]$^{4-}$

3.1. Mg$_2$FeH$_6$

The structural, spectroscopic and thermal characterization of Mg$_2$FeH$_6$ was first reported in 1984 by Didisheim et al [82]. The original objective for synthesizing this material was to prepare a material with greater hydrogen capacity than Mg$_2$NiH$_4$, by incorporating metals earlier in the *3d* series. In fact, Mg$_2$FeH$_6$ has a hydrogen volume 40 % greater than Mg$_2$NiH$_4$ as well has a greater theoretical hydrogen capacity of 5.6 wt% H compared to 3.6 wt% H.

The structure of Mg$_2$FeD$_6$ has been solved by simultaneous Rietveld refinement of X-ray and neutron diffraction data, with the material crystallizing in the *Fm−3m* space group with a K$_2$PtCl$_6$ structure type (Fig. 4a, Table 2) [82]. The D atoms occupy the 24*e* positions and are octahedrally coordinated around the Fe center at a distance of 1.556(5) Å, which is very similar to that of Mg$_2$NiD$_4$ (1.57 Å) [38] despite the tetrahedral configuration of the central Ni metal center in the latter. The Mg−D distances are determined to be 2.27 Å.
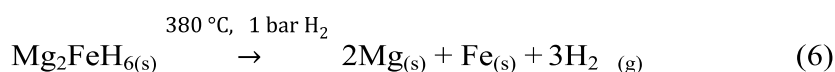
(Fig. 4)

The original synthesis of Mg_2FeH_6 reported sintering of elemental Fe and Mg powders in a 1:2 ratio, under a H_2 pressure of 120 bar at 450 – 520 °C, for up to 10 days (Eq. 5) [7]. Emphasis has centered on optimizing the synthesis method, including mechano-milling followed by sintering [83, 84]; reactive ball milling under an H_2 atmosphere without subsequent sintering [85, 86]; controlled reactive mechanical alloying (CRMA) [87]; and cryo-milling [88]. Although a two-step strategy was involved, one of the shortest times of synthesis has been reported by milling MgH_2 and Fe for 1 h at high energy prior to heat treatment under 100 bar H_2 for only 30 mins [83]. One of the lowest pressures utilized during the synthesis of Mg_2FeH_6 was 6 bar with the preparation of nanocrystalline Mg_2FeH_6 at room temperature after milling 3Mg + Fe for 100 h [89]. More recently, Mg_2FeD_6 was synthesized under 10 bar D_2 pressure at 360 °C for 48 h after milling MgD_2 and Fe powder for 12 h [90]. The need to synthesize high purity and large batches of material lead to the production of 20 g batches in a custom made reactor with yields of between 94 - 97 % at 120 bar H_2 with 2 h of milling [84].
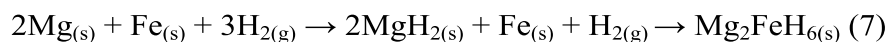
$$2Mg + Fe \quad \xrightarrow{450 - 520\ °C, \ 120\ bar\ H_2} \quad Mg_2FeH_6 \qquad (5)$$

The reported thermodynamics of hydrogen sorption of bulk Mg_2FeH_6 have been shown to vary considerably. ΔH has been reported as 98 ± 3 kJ/mol H_2 (desorption) [82], −86.6 ± 6 kJ/mol H_2 (absorption) [91] and −77.4 kJ/mol H_2 (absorption) [92]. These values also correlate very well to the value of −81.4 kJ/mol H_2 calculated using DFT [93]. ΔS_{des} has been reported as 147 ±9 J/K/mol H_2 [91] while a value of 134 J/K/mol was calculated from the desorption pressures reported by Bogdanović et al [92]. The discrepancy between these data sets is difficult to discern, although many factors can be attributed to poor collection of data. These factors have been discussed extensively in reference [94] and the associated supplementary information. In the case of Mg_2FeH_6, the ΔH value of −77.4 kJ/mol H_2 is deemed the most reliable as negligible hysteresis was observed between the absorption and desorption data. This suggests that equilibrium was achieved at each step in the PCT curves and multiple data points were collected over the pressure equilibrium plateau [92]. In addition, data was collected for five temperatures between 350 and 525 °C.

The mechanism for the reversible hydrogenation of Mg_2FeH_6 has been studied by XRD, DSC and PCT measurements [92, 95]. *In-situ* powder XRD studies have shown that the decomposition process is a one-step process in which Mg and Fe are the only remaining crystalline material (Eq. 6). DSC measurements conducted under 1 bar H_2 indicate decomposition of Mg_2FeH_6 to the elements to be a single-step reaction, which begins at 380 °C with a maximum heat flow rate at 420 °C [95]. Similarly, GC analysis of Mg_2FeH_6 under flowing Ar enabled decomposition with a desorption maxima of 360 °C [96]. As one would expect, an applied H_2 backpressure during decomposition allows stabilization of the material by 20 °C.

$$Mg_2FeH_{6(s)} \quad \xrightarrow{380\ °C, \ 1\ bar\ H_2} \quad 2Mg_{(s)} + Fe_{(s)} + 3H_{2\ (g)} \qquad (6)$$

The hydrogenation pathway from Mg and Fe powder was first studied by thermovolumetric analysis and TEM (transmission electron microscopy), in which after the first absorption (350 °C, 20-12 bar H_2 pressure, 48 h) MgH_2 and Mg_2FeH_6 are identified [92]. Further cycling allows for 5.0 wt% H_2 desorption with a single endothermic signal at 349 °C. Hydrogenation of decomposed Mg_2FeH_6 (Mg + Fe) has also been studied by *in situ* XRD with a temperature ramp from room temperature to 500 °C, under 100 bar H_2 [95]. MgH_2 was observed to form at ~200 °C, before the formation of Mg_2FeH_6 at ~380 °C and is described as an intermediate during the reaction (Eq. 7). In the same study, high-pressure DSC measurements indicate absorption to commence at 300 °C with a peak temperature at 403 °C under 125 bar H_2 pressure.

$$2Mg_{(s)} + Fe_{(s)} + 3H_{2(g)} \rightarrow 2MgH_{2(s)} + Fe_{(s)} + H_{2(g)} \rightarrow Mg_2FeH_{6(s)} \ (7)$$

The identification of MgH_2 as an intermediate during *in situ* hydrogenation may be due to thermodynamic constraints imposed on the material during the temperature ramp under 100 bar H_2 [95]. MgH_2 is preferentially formed due to a lower ΔH_{des} of 74 kJ/mol H_2 [97], as Mg_2FeH_6 has a ΔH_{des} of 77.4 kJ/mol H_2 [92]. Although the difference in ΔH is small, MgH_2 will have faster kinetics of formation compared to Mg_2FeH_6 in that temperature range. One experiment that may truly establish the pathway of formation is to cycle Mg_2FeH_6 isothermally, while altering the pressure to promote sorption. At the same time, MgH_2 is not observed during decomposition as desorption begins at temperatures at which MgH_2 cannot exist under such a low hydrogen partial pressure. For instance, Mg_2FeH_6 begins to desorb at 380 °C under 1 bar H_2 [95], but MgH_2 requires ~11 bar H_2 back pressure to be stabilised at this temperature [97].

Due to the high stability of Mg_2FeH_6, it has been largely studied for technological implementation as a thermal storage material (TES). One such application is for the TES material in Concentrating Solar Thermal plants current targets lie at operation temperatures of up to 600 °C [32, 33]. Mg_2FeH_6 has a theoretical operating temperature range of 304-564 °C (for pressures between 1 and 150 bar H_2) [31], while it has been demonstrated to cycle up to at least 600 times, at temperatures of up to 550 °C [33, 92].

A variety of imaging studies have been conducted on Mg_2FeH_6 including, SEM (scanning electron microscopy), TEM, HR-TEM (high resolution-transmission electron microscopy), along with FIB (focused ion beam) and Energy-Loss Spectroscopy [86, 89, 95, 98-101]. In one particular microstructural examination, it was revealed that the synthesized Mg_2FeH_6 powder generally exhibits a duplex structure, that consists of plate-like particles larger than 1 mm in diameter and spherical particles smaller than 50 nm, that show a tendency to agglomerate and form larger particles exhibiting a sponge-like structure. The formation of Mg_2FeH_6 takes place at the phase boundary between Fe seeds and the growing hydride phase. In contrast, the decomposition of the Mg_2FeH_6 phase takes place with the formation of the separate nano-sized Mg and Fe phases [83]. The stability of the Mg_2FeH_6 structure has been established by *in situ* XRD experiments conducted between 25 and 400 °C and under pressures of up to 36.5 GPa. Results show that the cubic structure is stable throughout this temperature and pressure range. A separate experiment shows that the bulk modulus of this material is 75.4(4) GPa and is comparable to the calculated value of 76.3 GPa [102].

FT-IR spectroscopy measurements on Mg_2FeH_6 indicate a single strong vibration at 1720 cm^{-1}, which shifts to 1262 cm^{-1} for the deuteride [103]. Raman spectroscopy shows a similar result with a medium vibrational band at 1870 cm^{-1}, which shifts to 1340 cm^{-1} on deuteration. In the same study, INS is used to compliment the FT-IR and Raman measurements. In conjunction with Mössbauer spectroscopy, the Fe is determined to exist in a low spin Fe(II) configuration. The DFT calculated values also corroborate these values and indicates that there should be a total of four observable Raman vibrations and three IR vibrations [104].

Although experimental determination of the electronic band gap values are not available, DFT calculations have established that Mg_2FeH_6 is a direct semiconductor with a GGA gap value of 1.96 eV [104], which also agree well with other calculated values [105, 106]. First principals DFT calculations were used to determine the electronic structure for Mg_2FeH_6 and showed that the valence states consist of nine electronic bands [93]. By partial DOS analysis, Miwa et al. suggest that the contribution of Mg orbitals is negligible. The lowest six bands, which lie from −9.5 to −1.7 eV, are mainly composed of H-1s orbitals, Fe-3d orbitals split into t_{2g} and e_g states due to the octahedral crystal-field, and the former forms the remaining three valence bands.

3.2. $[FeH_6]^{4-}$ Analogues

Unlike $[NiH_4]^{4-}$, $[FeH_6]^{4-}$ is capable of forming complexes with other metals without Mg^{2+} as one of the corresponding counterions. A variety of $M_2[FeH_6]^{4-}$ complexes have been reported in the literature, including M = Ca, Sr and Eu [105]. Ca_2FeD_6, as anticipated, also crystalizes in the cubic $Fm-3m$ space group, albeit with extended Fe−D bond distances of 1.62 Å (Table 2) [105]. Although neutron diffraction was not conducted on the Sr and Eu analogues, the calculated H positions determined Fe−H bond distances to be 1.683(2) Å and 1.648(5) Å, respectively. The elongation of the M−H(D) bond can be partially ascribed to the larger ionic radius and lower electronegativity of the Ca^{2+} (1.00 Å), Sr^{2+} (1.18 Å) and Eu^{2+} (1.17 Å) compared to Mg^{2+} (0.72 Å) [73, 107].

The electronic structures of Ca_2FeH_6 and Sr_2FeH_6 are deemed quite similar to that of Mg_2FeH_6 except for a narrowing of the valence bandwidths. This narrowing is most likely due to their larger lattice constants, which weaken the interaction between neighboring $[FeH_6]^{4-}$ complexes [93]. The densities of states obtained for these alkaline-earth compounds agree well with those of the previous theoretical study using local density approximation [105], in which it has been suggested that the ionic bonding character is entirely dominant.

Analogous to $[NiH_4]^{4-}$, quaternary compounds of $[FeD_6]^{4-}$ stabilized by quasi-isolated H$^-$ have been determined. MMg_2FeD_8 complexes (M = Ba, Sr and Eu) have a limiting ionic formula of $M^{2+} \cdot 2Mg^{2+} \cdot 2H^- \cdot [FeH_6]^{4-}$) and are structurally similar to their cubic M_2FeD_6 counterparts despite the insertion of additional H$^-$ anions[24, 108].The cations in the trigonal quaternary mixed metal complexes form elongated cubes that consist of six equatorial Mg^{2+} and two apical M^{2+} (Fig. 4b). The Fe−D bond distances in the mixed metal complexes are very similar to that of Mg_2FeD_6 (1.58 Å for Ba and Sr) suggesting that the Mg^{2+} has a greater influence in bond length than M. The main difference between these compounds is observed in the M−D bonds with the Ba analogue having

the largest distance of 2.74 Å, while Sr has a bond length of 2.66 Å, in accordance to ionic radii (Sr = 1.18 Å, Ba = 1.35 Å) [107].

Other iron-based quaternary metal hydride with $[FeD_6]^{4-}$ central moieties and quasi-isolated D^- anions include $Ca_4Mg_4Fe_3H_{22}$ and $Yb_4Mg_4Fe_3H_{22}$, which crystallize in the cubic space groups $P-43m$ and $P4/mmm$, respectively [21, 22]. The bond distances of these complexes are very similar to one another, with four Fe−D distances of 1.586(5) Å and two Fe−D distances of 1.554(7) Å in $Yb_4Mg_4Fe_3H_{22}$, while there are four Fe−D distances of 1.583(3) Å and two Fe−D distances of 1.563(5) Å in $Ca_4Mg_4Fe_3H_{22}$ (Fig. 4c and d). On average, these distances are significantly longer than those in Mg_2FeD_6 1.556(5) Å but shorter than those in $SrMg_2FeD_8$ (1.578(4) Å) and Ca_2FeD_6 (1.62 Å) [7, 24, 71, 108]. Again, the distances are in agreement with ionic size considerations. In these classes of materials, the D atoms are tetrahedrally coordinated by one Mg and three M atoms.

$Na_2Mg_2FeD_8$ was determined to crystalize in the orthorhombic space group $Pbam$, where the $[FeD_6]^{4-}$ is surrounded by a cubic array of four Mg^{2+} and four Na^+ cations [26]. There are two different Fe−D bond distances within the octahedral array with the two apical bonds being 1.610(9) Å and 1.592(6) Å for the four equatorial Fe−D bonds. The cubes of cations are connected in an edge-sharing two-dimensional network forming layers along the a/c plane, with a sheet of D^- atoms occupying the $4h$ sites in between. As such, the D^- is enveloped by a distorted octahedral array, consisting of four Na^+ and two Mg^{2+}. This is a rare feature, as the coordination of the D^- by M^+ and/or M^{2+} within complex transition metal hydrides has previously been determined to be predominately tetrahedral ($Na_2Mg_2NiH_6$ [69], $LaMg_2NiH_7$ [72], $SrMg_2FeH_8$ [108], $BaMg_2FeH_8$ [24], $Ca_4Mg_4FeH_8$ [21], $LaMg_2PdH_7$ [109, 110]), linear or trigonal bipyramidal configurations ($LiMg_2RuH_7$, Mg_3MnH_7) [4].

To date, there have been only two $[FeH_6]^{4-}$ complexes synthesized without the incorporation of an alkaline earth metal. The synthesis of $YLiFeH_6$ was achieved under hydrogen pressures of 6.1 GPa at 900 °C [111]. This combination of cations satisfies charge requirements of the tetravalent $[FeH_6]^{4-}$ anion, i.e. Li^+ and Y^{3+}. This compound crystallizes in the space group $F-43m$ with a lattice constant of 6.651 Å. The calculated Fe−H distance of 1.581 Å is longer than that of Mg_2FeH_6, and is corroborated by the observance of the Fe−H stretching mode by Raman spectroscopy at 150 cm^{-1} lower than that of Mg_2FeH_6. This compound is metastable and decomposes at room temperature and pressure.

Similar to $YLiFeH_6$, Li_4FeH_6 has also been synthesized at elevated temperatures and pressures with full formation being observed at 6.1 GPa of H_2 pressure at 900 °C [112]. Synchrotron X-ray powder diffraction data could be collected at ambient pressures and temperature with only partial decomposition of the sample. The experimental lattice parameters corroborated those calculated by DFT with Li_4FeH_6 crystallizing in a rhombohedral space group, $R-3c$, with a = 7.970(3) and c = 9.763(6) Å. Unfortunately, no calculated Fe−H bond distances have been presented. From the experimentally obtained compression curve, the bulk modulus of Li_4FeH_6 was calculated to be 35 ± 3 GPa, which was consistent with the theoretically obtained value of 35 GPa calculated at 9.7 GPa.

Of the $[FeH_6]^{4-}$ analogues, only the vibrational spectra of $Na_2Mg_2FeH(D)_6$, $YLiFeH_6$ Li_4FeH_6 and Ca_2FeD_6 have been measured, each with the corresponding DFT calculations also being reported [8, 26, 111, 113]. $Na_2Mg_2FeH_6$ was studied by FT-IR spectroscopy and its deuteride analogue studied by Raman spectroscopy [26]. Due to the complicated structure of this compound (space group *Pbam*, Z = 2), compared to the relatively simple M_2FeH_6 analogues (space group *Fm*-3*m*, Z = 4), the requirement for these complementary spectroscopic techniques to be corroborated by DFT calculations can easily be realized due to the total of 75 optical Γ-phonon modes. The FT-IR spectrum of $Na_2Mg_2FeH_8$, shows a multiplet of strong vibrational bands between 1752 and 1274 cm^{-1}. With the assistance of the DFT calculated frequencies, the peaks at 1752 and 1645 cm^{-1} are assigned to the octahedral Fe−H stretching vibrations, while the peaks at 1416 and 1274 cm^{-1} are attributed to the vibrational modes of the H$^-$ anions. The octahedral Fe−H(D) and isolated H(D)$^-$ vibrational modes are also easily distinguished in the Raman spectra of the $Na_2Mg_2FeH_8$ and deuteride analogue. For the hydride analogue, peaks at 1874, 1765 and 1732 cm^{-1} are attributed to the Fe−H stretching modes, while one H$^-$ vibrational mode is observed at 1412 cm^{-1}. One Fe−H bending mode is observed at 1076 cm^{-1}. The Raman spectrum for $Na_2Mg_2FeD_8$ is very similar to its hydride counterpart despite the expected isotopic shift of $\sqrt{2}$ [26].

$YLiFeH_6$ was studies by Raman spectroscopy with two vibrational modes being observed at 1080 and 1720 cm^{-1} [111]. A total of 24 optical Γ-phonon modes were calculated by DFT of which only the A_1 and E modes are Raman active, the T_2 modes are both Raman and infrared active, and the remaining T_1 modes being inactive in both Raman and infrared. The Fe−H stretching mode at 1720 cm^{-1} is 150 cm^{-1} lower than that observed for Mg_2FeH_6 (1786 cm^{-1}), but 145 cm^{-1} greater than $Na_2Mg_2FeH_8$ (1575 cm^{-1}) [26]. This directly corresponds to the Fe−H bond distances of the materials with the measured Fe−D bond distance being 1.556(5), 1.581 and 1.592(6) Å for Mg_2FeD_6, $YLiFeH_6$ (calculated) and $Na_2Mg_2FeD_8$, respectively [26, 82, 111]. Although the comparison is being made for Fe-H for FT-IR spectroscopy and Fe-D for bond distance, the same correlation would be expected if the H positions could be precisely determined by powder XRD. The electronic properties of $Na_2Mg_2FeH_6$ and $YLiFeH_6$ have also can calculated by DFT in refs [28] and [111], respectively.

3.3. Thermal Stability of $[FeH_6]^{4-}$ Analogues

The thermal stability Mg_2FeH_6 is greater than that of the Ni analogue with a ΔH_{des} of 77 kJ/mol H$_2$ compared to (64 kJ/mol H$_2$) [13, 92]. The decomposition products are Mg and Fe in contrast to Mg_2Ni for Mg_2NiH_4. In contrast to Mg_2FeH_6, $SrMg_2FeH_8$ and $BaMg_2FeH_8$ decompose into elemental Fe and unknown phases at about 440 °C and 450 °C, under 1 bar H$_2$ pressure, respectively [24, 108]. Both of these hydrides show greater stability than $Ca_2Mg_4Fe_3H_{22}$ (about 395 °C at 1 bar H$_2$) and $Yb_4Mg_4Fe_3H_{22}$ (~420 °C at 1 bar H$_2$) [21, 22]. ΔH_{des} of $Yb_4Mg_4Fe_3H_{22}$ was measured to be 137(3) kJ/mol H$_2$), which is slightly larger than that of $Ca_4Mg_4Fe_3H_{22}$ (122(4) kJ/mol H$_2$). These enthalpies are 50 % more stable than that of the ternary hydride Mg_2FeH_6 (77 kJ/mol H$_2$). These values correspond to the thermal stability of the binary hydrides as previously noted in the $[NiH_4]^{4-}$ complexes. The decomposition products are YbH, elemental Mg and Fe whereas $Ca_4Mg_4Fe_3H_{22}$ decomposes via Ca_2FeH_6, Fe, and Mg.
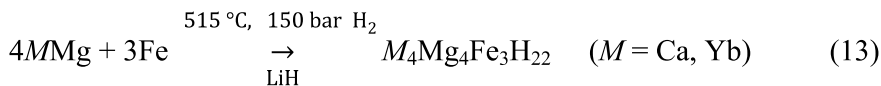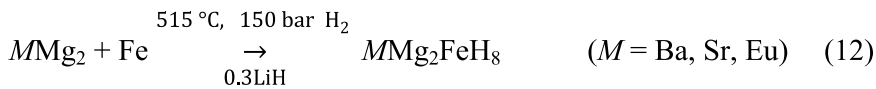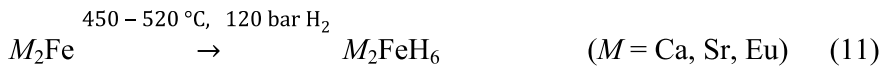
Li_4FeH_6 and $YLiFeH_6$ are only metastable and will decompose at room temperature and pressure [111, 112]. This is unsurprising considering that the average electronegativity of Li^+ and Y^{3+} is 1.04 (Allred Rochow scale). This is much less than that of complexes containing Mg^{2+} (1.24). As a result, $YLiFeH_6$ is deemed to be on the cusp of the lowest electronegativity required to stabilize the $[FeH_6]^{4-}$ anion [73]. On the same note, the Li^+ in Li_4FeH_6 has average electronegativity of 0.99, and as such is expected to be less stable than $YLiFeH_6$. DFT calculations estimate the standard formation enthalpy of Li_4FeH_6 to be −20 to −30 kJ/mol H_2 [112].

$Na_2Mg_2FeH_8$ decomposes in a three-step process via $NaMgH_3$ and NaH with the first desorption maxima occurring at *ca.* 400 °C under Ar flow (Eqns 8 - 10) [96]. PCI measurements determined the first stage occurs at 55 bar H_2 at 360 °C and has an associated ΔH_{des} = 93 kJ/mol H_2, while the second stage occurs at 0.5 bar H_2 (360 °C, ΔH_{des} = 87 kJ/mol H_2), whereas the final stage occurs at 0.1 bar H_2 (360 °C, ΔH_{des} = 87 kJ/mol H_2).

$$Na_2Mg_2FeH_8 \rightarrow 2NaMgH_3 + Fe + H_2 \qquad (1.3\ wt\%) \quad (8)$$

$$2NaMgH_3 + Fe \rightarrow 2NaH + 2Mg + 2H_2 + Fe \quad (2.5\ wt\%) \quad (9)$$

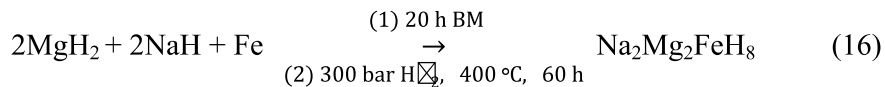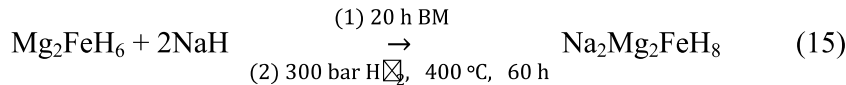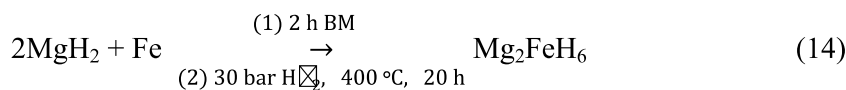$$2NaH + 2Mg + Fe \rightarrow 2Na + 2Mg + Fe + H_2 \quad (1.3\ wt\%) \quad (10)$$

3.4. Synthesis of $[FeH_6]^{4+}$ complexes

The synthesis of Mg_2FeH_6 and the analogous complexes is relatively simple and follows that of the $[NiH_4]^{4-}$ complexes. For $MgFeH_6$, Fe and Mg powders are sintered in a 1:2 ratio under a H_2 pressure of 120 bar at $450 - 520$ °C for up to 10 days (Eq. 5) [7]. For M_2FeH_6 complexes (M = Ca, Sr, Eu) the reaction is carried out under the same conditions, although the desired MFe alloy is prepared by arc melting prior to hydrogenation (Eq. 11) [9]. The yields from the synthesis of the Ca, Sr and Eu analogues are not as high as the Mg_2FeH_6 complex. The quaternary $[FeH_6]^{4-}$ complexes are synthesized by heating the corresponding MMg_2 alloy for MMg_2FeH_8 (M = Ba, Sr and Eu) or MMg alloy for $M_4Mg_4Fe_3H_{22}$ (M = Ca, Yb) with Fe and LiH powder at ~515 °C with 150 bar H_2 for two weeks (Eq. 12 and 13) [21, 22, 24, 108]. LiH aids yield of the synthesis. The black $Yb_4Mg_4Fe_3H_{22}$ product is stable in air for several weeks.

$$M_2Fe \xrightarrow{450-520\,°C,\ 120\,bar\ H_2} M_2FeH_6 \qquad (M = Ca,\ Sr,\ Eu) \quad (11)$$

$$MMg_2 + Fe \xrightarrow[0.3LiH]{515\,°C,\ 150\,bar\ H_2} MMg_2FeH_8 \qquad (M = Ba,\ Sr,\ Eu) \quad (12)$$

$$4MMg + 3Fe \xrightarrow[LiH]{515\,°C,\ 150\,bar\ H_2} M_4Mg_4Fe_3H_{22} \quad (M = Ca,\ Yb) \qquad (13)$$

$Na_2Mg_2FeH_8$ has been demonstrated to be synthesised by two methods, either a two-step synthesis involving the formation of Mg_2FeH_6 followed by reaction with NaH can be employed, or by hydrogenation of a stiochiometric mixture of NaH, MgH_2 and Fe (Eq. 14-16). Both of these reactions require 400 °C and 300 bar H_2 [96].

$$2MgH_2 + Fe \xrightarrow[\text{(2) 30 bar H}_2,\ 400\,°C,\ 20\,h]{\text{(1) 2 h BM}} Mg_2FeH_6 \qquad (14)$$

$$Mg_2FeH_6 + 2NaH \xrightarrow[\text{(2) 300 bar H}_2,\ 400\,°C,\ 60\,h]{\text{(1) 20 h BM}} Na_2Mg_2FeH_8 \qquad (15)$$

$$2MgH_2 + 2NaH + Fe \xrightarrow[\text{(2) 300 bar H}_2,\ 400\,°C,\ 60\,h]{\text{(1) 20 h BM}} Na_2Mg_2FeH_8 \qquad (16)$$

4. Complexes of $[CoH_5]^{4-}$

4.1. Mg_2CoH_5

Mg_2CoH_5 possesses a high volumetric and gravimetric hydrogen density (~100 kg H_2/m^3 and 4.5 wt.%, respectively) [114]. Structurally, Mg_2CoH_5 is reported to form two allotropes, one that exists at room temperature and another above 207 °C. At room temperature, the $[CoH_5]^{4-}$ anion in Mg_2CoH_5 exists as a tetragonally distorted CaF_2-type structure with a space group *P4/nmm* (Fig. 5a,b and Table 3) c. In this arrangement, the Co is surrounded by a square-pyramidal array of five hydrogen atoms. From neutron diffraction experiments of the deuteride analogue, the Co−D distances at the base are 1.515(3) Å, while the apical D is a significantly longer 1.590(17) Å, as expected for a d^8 system with C_{4v} symmetry. These bond distances are consistent with the *T*−D distance observed for analogous Mg_2FeD_6 (1.556 Å)[82] and Mg_2NiD_4 (1.56 Å)[47] systems. The $[CoH_5]^{4-}$ complex anion is surrounded by four Mg^{2+} ions, with Mg−D distances of 2.17 − 2.40 Å [115]. When heated above 207 °C, a phase modification occurs, where the structure is arranged in a distorted cubic space group of *Fm−3m*. A disordered distribution of D atoms is observed around the central Co atom, similar to that in high temperature phase of Mg_2NiD_4 [53], with a statistical distribution of five D's over six sites [115]. Conductivity and DSC measurements indicate the phase transition to be reversible with $\Delta H = 2.1$ kJ/mol [116].

Various thermal experiments have been conducted to ascertain the enthalpy of formation and decomposition of Mg_2CoH_5. PCT analysis by Zolliker et al. showed hysteresis between absorption and desorption measurements with a ΔH_{des} 86(5) kJ/mol H_2 and ΔH_{abs} −60(5) kJ/mol H_2, giving an average of 73(5) kJ/mol H_2 [115]. Further studies by Ivanov et al. determined ΔH_{des} for a 'low pressure' and a 'high pressure' phase by PCT measurements [116]. The 'high pressure' phase was deemed to have a ΔH_{des} of 79 ± 4 kJ/mol H_2 and ΔS_{des} of 134±4 J/K/mol H_2 and was determined to have the same tetragonal structure as reported by Zolliker et al [115]. In addition, the resistivity of Mg_2CoH_5 was determined to be in the order of $10^8 − 10^9$ μΩ at room temperature, consistent with the assumption of nonmetallic behavior [115].

In a study by Ivanov et al, the 'low pressure' phase was alluded to crystallize in an hexagonal space group [116], although the structure was finally solved by Cérny et al. [6] to be γ-$Mg_6Co_2H_{11}$. A joint synchrotron and neutron diffraction study along with *ab initio* calculations deduced the structure to be similar to Mg_2CoH_5, although along with the $[CoH_5]^{4-}$ complex anions, saddle like

$[CoH_4]^{5-}$ ions are also present (Fig. 5c) [6]. In total, there are 14 symmetrically independent hydrides, nine are bound to the Co metal centers (both of which occupy $8d$ positions), with distances ranging from 1.52(1) to 1.62(2) Å. The remaining five hydrides reside on a mirror plane, of which four are coordinated by four Mg atoms in a saddle-like configuration, and one has a triangular magnesium coordination.

Other than the reported structural studies of $Mg_6Co_2H_{11}$, further reports detail that this compound will transform into the tetragonal Mg_2CoH_5 phase if kept under 20 bar of hydrogen pressure for two days at 227 °C. In addition, the thermodynamics of this phase transition event has been determined to have a ΔH_{des} of 70 ± 4 kJ/mol H_2 and ΔS_{des} of 118±4 J/K/mol H_2 [116]. The phase change to the tetragonal phase has been shown to cause an increase in conductivity [116], while the transition to the cubic phase also exhibits an increase in conductivity [115].

A recent study by Norek et al. investigated the thermal decomposition and hydrogenation of Mg_2CoH_5 by *in situ* XRD and analyzed by SEM and high resolution STEM (scanning-transmission electron microscopy) [117]. The formation of Mg_2CoH_5 from a MgH$_2$-Co mixture under 85 bar H_2 pressure was observed to proceed in less than 2.5 h, with a yield of ~90 % at 300 °C. The irregularly shaped, nanostructured Mg_2CoH_5 particles have a porous appearance and an average size of 5 nm. Decomposition was observed to occur at approximately 360 °C, with the formation of elemental Mg and Co, which react to form intermetallic MgCo at ~400 °C. SEM and STEM imaging of this material identified that the morphology of the particles had not significantly altered, although BF-STEM (bright field scanning-transmission electron microscopy) imaging identified dark precipitates on a bright matrix, indicative of MgCo surrounded by a matrix of Mg. The resultant mixture was then subjected to the same conditions as the preliminary hydrogenation. MgH$_2$ was observed to form at >100 °C, followed by the formation of cubic Mg_2CoH_5 at 300 °C. The activation energy of decomposition, identified by DSC, was determined to be 114.8 kJ/mol [117].

4.2. $[CoH_5]^{4-}$ Analogues

Recent variations of these 18-electron quaternary hydride systems include a mixed complex ion system with the formula $Mg_2(FeH_6)_{0.5}(CoH_5)_{0.5}$ synthesized by Deledda et al [118]. This material can be synthesized either by milling the elemental powders under 50 bar H_2 or D_2 or milling the individual constituents (Mg_2FeH_6 and $MgCoH_5$) under an Ar atmosphere. The product assumes a cubic K_2PtCl_6-type structure, commonly observed for these systems, and was determined by powder neutron and XRD diffraction to possess a unit cell of $a = 6.42$ Å. The Fe and Co are randomly distributed in the $4a$ position and D in the $24e$ positions, with an average transition metal to D bond distance of 1.525 Å. This material has a volumetric hydrogen capacity of 138 g/L and a gravimetric capacity of 4.8 wt% H_2. During TPD measurements, hydrogen is desorbed in a single step, commencing at 227 °C, with a maximum value at 297 °C. This value is an average of that measured for the constituent Mg_2TH_x, which have maxima at 287 and 312 °C for $[FeH_6]^{4-}$ and $[CoH_5]^{4-}$, respectively. The desorption products, determined by *in situ* XRD are Mg and a FeCo solid solution. This system was investigated further by INS and periodic-DFT calculations in order to fully understand the vibrational spectrum of the material, with periodic DFT aiding the identification of the individual vibrational modes [119].
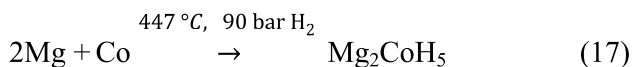
Shelyapina et al. calculated the electronic structure of $Mg_2(FeH_6)_{0.5}(CoH_5)_{0.5}$, Mg_2FeH_6 and Mg_2CoH_5 by the FLAPW method to understand the relative stabilities of the compounds [120]. The enthalpies of formation were calculated to be -145.2, -156.2 and -148 kJ/mol H_2 for Mg_2FeH_6, $MgCoH_5$ and $Mg_2(FeH_6)_{0.5}(CoH_5)_{0.5}$, respectively. Although, these values are inflated compared to the reported experimental values, they do emphasize that the properties of $Mg_2(FeH_6)_{0.5}(CoH_5)_{0.5}$ are an intermediate between the two parent molecules. The theoretical calculations also determined that $Mg_2(FeH_6)_{0.5}(CoH_5)_{0.5}$ is nonmagnetic.

Except for Mg_2CoH_5, only three other complexes of $[CoD_5]^{4-}$ are reported in the literature, $Sr_4Mg_4Co_3H_{19}$, $Ca_4Mg_4Co_3H_{19}$ and $Yb_4Mg_4Co_3H_{19}$ [25, 121]. These complexes are isomorphous to the $[FeH_6]^{4-}$ complexes of $M_4Mg_4Fe_3H_{22}$ (M = Ca, Yb) [21, 22], differing only by the occupancy of the apical transition metal hydride, in which it is only half occupied in the Co analogue and fully occupied in the Fe compounds. As with Mg_2CoD_5, the apical Co−D bonds (1.586(9) and 1.58(1) Å for Ca and Yb, respectively), are greater than the equatorial equivalents (1.546(3) and 1.546(5) Å for Ca and Yb, respectively). The quasi-isolated deuteride anions are tetrahedrally coordinated by one Mg (1.912(5) Å (Ca) and 1.907(7) Å (Yb)) and three M^{2+} (2.355(6) Å (Ca) and 2.354(5) Å (Yb)), all of which are shorter than the $[FeD_6]^{4-}$ counterparts.

The thermal stability of $Ca_4Mg_4Co_3H_{19}$ is such that decomposition occurs at 480 °C under 5 bar H_2 to CaH_2, Co and Mg [25]. This decomposition pathway is in contrast to that of the analogous $Ca_4Mg_4Fe_3H_{22}$ which decomposes into Ca_2FeH_6, Mg and Fe [22]. As the electronegativity of Ca^{2+} is much lower than Mg^{2+} it is not able to stabilize the $[CoH_5]^{4-}$ anion and as such will not form Ca_2CoH_5 or even $CaMgCoH_5$ [73]. As such it decomposes into the binary hydride as is observed with the analogous $Yb_4Mg_4Fe_3H_{22}$ compound [22].
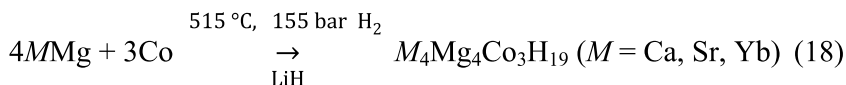
4.3. Synthesis of $[CoH_5]^{4-}$ complexes

The synthesis of Mg_2CoH_5 was originally conducted using similar conditions to that of Mg_2FeH_6, with sintering of the elemental metals at 90 bar H_2 at temperatures between 447 and 497 °C (Eq. 17) [17, 122]. To reduce the reaction conditions, Huot et al. ball milled the Co and Mg starting materials in an argon atmosphere (1 bar) and hydrogen (10 bar) followed by sintering under hydrogen [123]. This allowed the synthesis conditions to decrease to a more moderate 350 °C and 50 bar H_2. Despite the moderate conditions, a yield of < 30 % Mg_2CoH_5 was identified by XRD after reactive milling under Ar or H_2.

$$2Mg + Co \xrightarrow{447\,°C,\ 90\ bar\ H_2} Mg_2CoH_5 \qquad (17)$$

$Mg_6Co_2H_{11}$ was synthesized by mixing Mg and Co in a 2:1 ratio before pressing the powder in to pellets [6]. The pellets were then annealed at 480-500 °C for 24 h under 40-50 bar H_2 pressure. The large unreacted Mg grains were then removed by passing the powder through a sieve and the Co was removed using a magnet. Its synthesis has also been demonstrated to occur by heating Mg and Co powders in a 2:1 ratio between 417 and 437 °C at 20 bar H_2 [116].

The $M_4Mg_4Co_3H_{19}$ (M = Ca, Sr, Yb) compounds were synthesized in a similar fashion to their Fe counterparts, with the elemental metals being treated by arc melting, followed by sintering at ~527 °C and 155 bar H_2 (Eq. 18) [25]. LiH was also added to enhance the yield of the reaction. They were found to crystalize in the cubic space group $P-43m$.

$$4M\text{Mg} + 3\text{Co} \xrightarrow[\text{LiH}]{515\,°C,\ 155\ \text{bar}\ H_2} M_4Mg_4Co_3H_{19}\ (M = \text{Ca, Sr, Yb})\quad (18)$$

5. Complexes of $[RuH_6]^{4-}$

5.1. Mg_2RuH_6

Mg_2RuD_6 was first reported in 1991, with the Ru metal center observing the 18-electron rule as with the $[NiH_4]^{4-}$, $[CoH_5]^{4-}$ and $[FeD_6]^{4-}$ complexes [9]. The material is synthesized by the sintering of Ru and Mg in a 1:2 ratio under a H_2 pressure of 85 bar at 450 °C for up to 10 days, with a total yield of 95 % (Eq. 19).

$$2\text{Mg} + \text{Ru} \xrightarrow{450\,°C,\ 85\ \text{bar}\ H_2} Mg_2RuH_6 \quad (19)$$
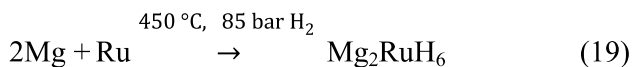
Neutron diffraction of the deuterated analogue determined that the material crystalizes in a cubic space group of $Fm-3m$, with a K_2PtCl_6 structure type (Fig. 6a and Table 4) [9]. As with Mg_2FeD_6, the Ru is octahedrally coordinated by D with a bond distance of 1.673(4) Å, which is longer than that of the Fe congener of 1.556(5) Å [82] (as expected from the increased ionic radii of the metal center). Along with the increase in Ru−D bond length is a concomitant expansion of the unit cell. Mg_2FeD_6 has the lattice parameter a = 6.430(1) Å while Mg_2RuD_6 has a = 6.6294(8) Å, an expansion of 3 %. The Mg−D distance in this compound is determined to be 2.3439(2) Å, which is longer than that of the Fe congener of 2.2739(3) Å [7].

(Fig. 6)
(Table 4)

5.2. $[RuH_6]^{4-}$ Analogues

Unfortunately, there is a dearth of reports on the physical characterization of $[RuH_6]^{4-}$ as compared with $[NiH_4]^{4-}$, $[FeH_6]^{4-}$ and $[CoH_5]^{4-}$ analogues, but $[RuH_6]^{4-}$ does have a rich structural chemistry and forms a variety of hydride complexes. Moyer et al. have reported a number of M_2RuH_6 (M = Ca, Eu, Sr and Yb) compounds and their deuterated analogues [12, 15, 16, 124-127]. This class of compounds crystallizes in the $Fm-3m$ space group (Table 4). The lattice parameters of these complexes are again significantly larger than the analogous $[FeH_6]^{4-}$ complexes. The Ru−D bond distance in Ca_2RuD_6 (1.700(2) Å) is comparable to the Ru−D distance in Mg_2RuD_6 (1.673(4) Å), although the M−D distances are significantly different (Ca−D = 2.5553(1) Å, Mg−D = 2.34 Å) [9, 126]. The cause of this difference is the ionic radii of the metals with Ca^{2+} being 1.00 Å and Mg^{2+} being 0.72 Å [107].

Unlike $[NiH_4]^{4-}$ and $[FeD_6]^{4-}$, $[RuD_6]^{4-}$ is able to be stabilized by monovalent alkali metals only to form A_4RuH_6 (A = Li and Na) complexes [11]. These materials crystallize in a rhombohedral, K_4CdCl_6 type, structure in space group $R-3c$ (167). The structure can be described by isolated $[RuH_6]^{4-}$ ions located in a cube of alkali metal ions (Fig. 6b). Two types of A^+ counterions have been distinguished within the structure, $A^+(1)$ links the octahedral $[RuH_6]^{4-}$ groups together to form chains in the c-direction, and $A^+(2)$ is inserted in the spaces between the chains. The $A^+(1)$, located in position $6a$, has a distorted trigonal prism of hydrogen atoms as nearest neighbors at a distance of 2.352(9) Å in Na_4RuD_6. The cubic alkali ion environment completely separates the anions from each other, which is a common feature of this type of hydride. With a Ru–H distance of 1.714(5) Å and 1.792(9) Å for Li and Na, respectively, it is noticeable that the Ru–H distance is sensitive to the size and thus the stabilizing effect of the counterion [11].

The experimental thermodynamic properties of MRuH$_6$ have not been established. A recent computational screening study by Nicholson and Sholl indicate that Eu_2RuH_6, Yb_2RuH_6, Ca_2RuH_6 and Ba_2RuH_6 have a ΔH_f of –189.5, –185.9, –175.0 and –157.7 kJ/mol H$_2$, respectively (Table 4) [35]. These values correlate very well with the ionic size and electronegativity of the M atom. These values also agree well with the DFT calculated values by Miwa et al of the $[FeH_6]^{4-}$ analogues (Table 2) [93]. The ΔH_f of –153.7 kJ/mol H$_2$ calculated for CaFeH$_6$ is 21.3 kJ/mol H$_2$ lower than that for Ca$_2$RuH$_6$, which is expected due to the extra stability provided by the Ru metal centre over the Fe metal centre.

Another parallel to the $[FeH_6]^{4-}$ system is the formation of MMg$_2T$H$_8$ compounds. Huang et al. successfully synthesized BaMg$_2$RuD$_8$ and revealed that the structure possess an alternate structure to that of BaMg$_2$FeD$_8$ [20, 24]. Although both complexes contain two types of hydrogen, (octahedrally coordinated to the T atoms and another tetrahedrally bonded to Ba and Mg only), their local symmetries differ significantly. In BaMg$_2$RuD$_8$, the complexes have tetragonal symmetry and are surrounded by four Mg and four Ba ions, which form two interpenetrating octhedra (Fig. 6c), similar to that in Ca$_4$Mg$_4$Fe$_3$D$_{22}$ (Fig. 4c and d) [21]. In BaMg$_2$FeD$_8$, the complexes have trigonal symmetry and are surrounded by an alkaline earth metal cube, consisting of six equatorial Mg and two apical Ba ions [24]. The difference can be attributed to the size requirements of the T atom. The H$^-$ ions also have an alternate configuration. In BaMg$_2$FeD$_8$ they are surrounded by two Mg and two Ba ions, whereas in the $[RuH_6]^{4-}$ analogue they are surrounded by one Mg and three Ba ions, with bond distances of 1.990(3) Å and 2.766(3) Å, respectively.

Na$_2$Mg$_2$RuH$_8$ crystalizes in the space group $Pbam$ and is isostructural to Na$_2$Mg$_2$FeH$_8$. The $[RuH_6]^{4-}$ anion is surrounded by a cube of two Mg and two Na atoms, as is the H$^-$ anion. The structure of Na$_2$Mg$_2$FeH$_8$ is described in more detail above. For Na$_2$Mg$_2$RuD$_8$, the Ru–D bond is 1.749(2) Å, which is 0.157 Å longer than Na$_2$Mg$_2$FeH$_8$ on account of the larger ionic radius transitional metal, while it is also longer than that of Mg$_2$RuH$_6$ on account of the electronegativity of the cations. PCI measurements have determined thermal decomposition to occur in a two-step process via the formation of Mg$_2$RuH$_4$ to Mg$_3$Ru$_2$, Na and H$_2$ under 0.5 bar H$_2$ pressure at 450 °C [96]. The enthalpies of decomposition associated with these events are 131 kJ/mol H$_2$ for step one

and 119 kJ/mol H_2 for the second. The overall enthalpy of decomposition is 125 kJ/mol H_2. Decomposition under reduced pressure allows for the onset of decomposition to occur at ca. 325 °C, with the first maxima being observed at ca. 421 °C, and the second at ca. 460 °C. Cycling of this material has not been conducted although the pressures of 300 bar are required for full synthesis of $Na_2Mg_2RuH_8$.

Another class of quaternary $[RuH_6]^{4-}$ complexes is that of $LiMg_2RuH_7$, which crystallizes in the hexagonal $P6_3/mmc$ space group [23]. The $[RuH_6]^{4-}$ complex is surrounded by six Mg and two Li cations in a cubic configuration (Fig. 6d). Within the structure, adjacent cubes are linked via Mg-Mg edges to sheets parallel to the hexagonal plane, and via lithium corners. This structural motif is similar to that observed in Mg_3RuD_6 and $SrMg_2FeD_8$ [108, 128]. The interstitial D^- anions are coordinated by two Mg^{2+} and three Li^+ in a trigonal bipyramidal array with Mg−D and Li−D bond distances of 1.852(6) Å and 2.7134(1) Å, respectively. $LiMg_2RuH_7$ decomposes between 570 - 580 °C, under a hydrogen pressure of ~70 bar, forming the ternary hydride Mg_2RuH_6 and LiH.

Extensive vibrational spectroscopy studies have been conducted on M_2RuH_6 (M = Mg, Ca, Ba, Yb, Sr and Eu) and Li_4RuH_6 (Table 4) [8, 14, 126, 127, 129-133]. Analysis includes Raman, FT-IR, inelastic neutron scattering and photoacoustic vibrational spectroscopies, with the use of DFT calculations to corroborate the data. The spectra of all the M_2RuH_6 analogues are very similar with six internal vibrations allowed for these high symmetry $[RuH_6]^{4-}$ complexes. The deuterated versions have an expected wave number ratio of $\sqrt{2}$. For instance, in the IR spectrum of Yb_2RuH_6, the Ru−H stretching vibration occurs at 1548 cm^{-1} for the hydride and 1110 cm^{-1} for the deuteride [127]. The authors confirm previous reports that the marriage of all methods of vibrational analysis permits the identification of all fundamental vibrations, which may be inactive by some methods [103, 132]. First-principles calculations and vibrational spectroscopy studies of Li_4RuH_6 have determined three peaks at approximately 215, 852, and 1795 cm^{-1} by Raman spectroscopy whereas the IR spectrum shows two peaks at approximately 574 and 1527 cm^{-1} [14].

The pressure dependency of the M_2RuH6 (M = Ca, Eu and Sr) compounds were studied by Raman spectroscopy up to a pressure of 5 GPa [129]. A phase change was not observed, although a linear increase in wavenumber was observed as pressure increased. The bulk moduli and mode Grüneisen parameters were derived by extrapolation of the data, with the bulk modulus being in the range of 18.8 and 12.9 GPa for Ca and Eu, respectively. Further studies by periodic density functional theory calculations performed at the local density approximation (LDA) and generalized gradient approximation (GGA levels) have further determined the bulk modulus of Ca_2RuH_6 to be 67.6 and 58.5 GPa, respectively [134]. The discrepancy between the extrapolated experimental and DFT results have been postulated to be due to the fact that the equivalence between chemical and physical pressures assumed for the experimental determination of the bulk modulus does not quantitatively hold for the ternary metal hydrides.

Static ^2H NMR spectroscopy was conducted on Yb_2RuD_6 and Ca_2RuD_6 [126, 127]. The spectra of both compounds showed a Pake doublet with a coupling constant of 54.7 and 40.9 kHz for Ca and Yb, respectively. The coupling constants have been shown to predict the degree of ionic character between a bond [126]. In this case, a value of 76 % for Ca and 82 % for Yb has been attributed to

the Ru−D bond. The larger value for Yb_2RuD_6 is indicative of a larger ionic character than the Ca analogue. This is in line with the shorter Ru−D bond for Ca (1.700(2) Å) than Yb (1.7223(19) Å) [126, 127].

6. Influence of Counter-cations on Transition Metal Complex Anion

Recent studies have reported general trends between the analogues of the transition metal, *T*, hydride complexes. Articles reporting the crystallographic structures of novel compounds often note a marked difference in *M*−H(D) bond lengths and have correctly attributed them to the varying ionic radius of the *M* atom. For instance, the Mg−D distance in Mg_2RuD_6 is 2.34 Å while the Sr−D distance in Sr_2RuD_6 is 2.69 Å, which correlates with the ionic radii of the metals being 1.18 Å for Sr^{2+} and 0.72 Å for Mg^{2+} [107]. This works well for complexes with mono-cation complexes although it is difficult to determine the average ionic radii for bi-cation complexes. Difficulties can often arise determining the specific ionic radius for a particular coordination number of a metal.

One recent DFT study calculated the thermodynamic stability of $(M, M')_2FeH_6$ (M, M' = Mg, Ca, and Sr) and compared them to some hypothetical complexes involving *M* = Mn and Zr [93]. It is deemed that the electronegativity of the cation elements is a good indicator to estimate the thermodynamical stability of M_2FeH_6 compounds. Plotting ΔH_f against electronegativity, using the Alled-Rochow scale, gives a direct linear correlation. A further study correlated the electronegativity of cation elements against ΔH_f of $(M, M')_4FeH_8$ complexes and investigated further hypothetical complexes such as *M* = Na, Li; *M'* = Mg, Zn, Y, Al [28]. These studies ultimately show that the thermodynamic stability is tuned by the average cation electronegativity and that these methods can predict the possibility of the formation of novel complexes.

The countercations (*M*) exhibit a strong influence over the anion complex and as such an inverse linear correlation has been established with *T*−D distance with the average electronegativity of *M* [73]. This is especially true for the 3*d* transition metal complexes of Fe, Co and Ni whereas little effect is exhibited by the 4*d* $[RuD_6]^{4-}$ complexes. The decreased effect on the Ru anion is due to the increased stabilization of the central metal atom attained by the spatially more extensive orbitals of Ru, which are able to overlap with greater effectiveness with the H 1*s* orbitals than the more compact 3*d* orbitals. This is responsible for the formation of a greater variety of $[RuD_6]^{4-}$ complexes [27, 73]. By assessing the average electronegativity of the countercations for known complexes, an experimentally determined threshold has been established for $[FeH_6]^{4-}$, $[CoH_5]^{4-}$ and $[NiH_4]^{4-}$ complexes and allows for the intuitive design of novel transition metal hydrides as well as the estimation of *T*−D bond lengths.

Several studies have focused on developing correlations involving the vibrational frequencies of complex transition metal hydrides. Kritikos and Noréus reported in 1991 on the nonlinear correlation with a decrease in wavenumber as the length of the unit cell (*a*) increases for the various $[RuH_6]^{4-}$ analogues [10]. As such the highest Ru−H asymmetric stretch in the FT-IR spectrum appears at 1783 cm^{-1} for Mg_2RuH_6 (*a* = 6.6561(3) Å), while νRu−H for Eu_2RuH_6 is at 1480 cm^{-1} (*a* = 7.556 Å) (Table 4) [10]. A correlation has also been observed between IR *T*−H stretching

frequencies with T–H bond length using Badger's rule [8, 14]. Although some discrepancies are observed, it is apparent that vibrational frequency of the T−H stretching band decreases with increasing bond length. Gilson and Moyer have also reported a linear relationship between the vibrational wavenumbers and the ionization potential of the counterion [135]. This relationship also provides quantitative support for the charge-transfer mechanism for explaining the stabilities of these compounds.

7. Conclusions and future aspects

The 18-electron hydride complexes of Ni, Fe, Co and Ru have been and continue to be studied over recent years, with the results identifying the rich chemistry and physical properties that these compounds boast. These properties behold this classification of materials to have a future in device applications, including Smart Optical Windows, energy storage materials in fuel cells for both stationary and mobile applications, and also as thermal energy storage materials in applications such as Concentrating Solar Thermal plants. For low temperature applications, the high thermal stability and slow kinetics of these compounds will pose a significant question over their particular effectiveness as an energy storage material, although the capability of reversible hydrogenation of these systems is a positive factor and one that will be continued to be considered. The addition of dopants and the combination of these materials with other hydrogen storage materials in binary reactive hydride composite systems has been studied, albeit outside the scope of this review, although it has been indicated that improved kinetics and thermodynamics have been observed. The ability to synthesize high purity material is also a problem as the theoretical hydrogen capacity is difficult to achieve.

The analysis of the ternary hydride systems has been carried out meticulously, including a number of XRD and neutron diffraction experiments, DFT calculations, NMR and vibrational spectroscopies. Thermal analysis of the compounds has been conducted by DSC, TGA, TPD and PCT measurements with the products of each stage being imaged by electron microscopy.

The synthesis of new analogues of these compounds has slowed since the vigorous emphasis in the 1980's and 1990's. The possibility to stabilize the T center of the $3d$ metals with anything other than Mg^{2+} counterion is problematic, with those that have been successfully synthesized having an extremely poor yield. Only a few quaternary complexes have been effectively produced, of which are mostly alkali-earth or doubly charged rare-earth metals. Increasing the combined charge of the cation leads to the formation of substances which incorporate ionic and covalent hydrides. There is a dearth of physical analysis of these compounds, with only the molecular structure having been determined. With further insight, these class of materials may behold some interesting characteristics including fast-ion conduction.

Acknowledgements

Notes and references

[1] G. Li, M. Matsuo, S. Deledda, R. Sato, B.C. Hauback, S.-i. Orimo, Mater. Trans., 54 (2013) 1532-1534.

[2] C. Pistidda, S. Garroni, F. Dolci, E.G. Bardají, A. Khandelwal, P. Nolis, M. Dornheim, R. Gosalawit, T. Jensen, Y. Cerenius, S. Suriñach, M.D. Baró, W. Lohstroh, M. Fichtner, J. Alloys Compd., 508 (2010) 212-215.

[3] A. Züttel, M. Hirscher, B. Panella, K. Yvon, S.-i. Orimo, B. Bogdanović, M. Felderhoff, F. Schüth, A. Borgschulte, S. Goetze, S. Suda, M.T. Kelly, Hydrogen as a Future Energy Carrier, Wiley-VCH Verlag GmbH & Co. KGaA, 2008.

[4] K. Yvon, Chimia, 52 (1998) 613-619.

[5] K. Yvon, G. Renaudin, Hydrides: Solid State Transition Metal Complexes, John Wiley & Sons, Ltd, 2006.

[6] R. Cerny, F. Bonhomme, K. Yvon, P. Fischer, P. Zolliker, D.E. Cox, A. Hewat, J. Alloys Compd., 187 (1992) 233-241.

[7] J.J. Didisheim, K. Yvon, P. Fischer, J. Schefer, M. Gubelmann, A.F. Williams, Z. Kristallogr., 162 (1983) 61-61.

[8] H. Hagemann, V. D'Anna, L.M. Lawson Daku, S. Gomes, G. Renaudin, K. Yvon, J. Phys. Chem. Solids, 72 (2011) 286-289.

[9] B. Huang, F. Bonhomme, P. Selvam, K. Yvon, P. Fischer, J. Less-Common Met., 171 (1991) 301-311.

[10] M. Kritikos, D. Noréus, J. Solid State Chem., 93 (1991) 256-262.

[11] M. Kritikos, D. Noréus, A.F. Andresen, P. Fischer, J. Solid State Chem., 92 (1991) 514-519.

[12] R.O. Moyer, J.S. Thompson, Abstr. Pap. Am. Chem. Soc., (1973) 125-&.

[13] J.J. Reilly, R.H. Wiswall, Inorg. Chem., 7 (1968) 2254-2256.

[14] T. Sato, S. Takagi, M. Matsuo, K. Aoki, S. Deledda, B.C. Hauback, S. Orimo, Mater. Trans., 55 (2014) 1117-1121.

[15] D.F. Storey, R. Lindsay, R.O. Moyer, Abstr. Pap. Am. Chem. Soc., 198 (1989) 174-INOR.

[16] J.S. Thompson, R.O. Moyer, R. Lindsay, Inorg. Chem., 14 (1975) 1866-1869.

[17] P. Zolliker, K. Yvon, P. Fischer, J. Schefer, Helv. Chim. Acta, 57 (1984) 754-754.

[18] S.F. Parker, Coord. Chem. Rev., 254 (2010) 215-234.

[19] J.-N. Chotard, Y. Filinchuk, B. Revaz, K. Yvon, Angew. Chem., 118 (2006) 7934-7937.

[20] B. Huang, F. Gingl, F. Fauth, A. Hewat, K. Yvon, J. Alloys Compd., 248 (1997) 13-17.

[21] B. Huang, K. Yvon, P. Fischer, J. Alloys Compd., 190 (1992) 65-68.

[22] B. Huang, K. Yvon, P. Fischer, J. Alloys Compd., 197 (1993) 65-68.

[23] B. Huang, K. Yvon, P. Fischer, J. Alloys Compd., 210 (1994) 243-246.

[24] B. Huang, K. Yvon, P. Fischer, J. Alloys Compd., 227 (1995) 121-124.

[25] B. Huang, K. Yvon, P. Fischer, J. Alloys Compd., 227 (1995) 116-120.

[26] T.D. Humphries, S. Takagi, G. Li, M. Matsuo, T. Sato, M.H. Sørby, S. Deledda, B.C. Hauback, S. Orimo, J. Alloys Compd., 645 (2015) S347–S352.

[27] K. Kadir, D. Noréus, Inorg. Chem., 46 (2007) 3288-3289.

[28] S. Takagi, T.D. Humphries, K. Miwa, S. Orimo, Appl. Phys. Lett., 104 (2014) 203901.

[29] B. Farangis, P. Nachimuthu, T.J. Richardson, J.L. Slack, B.K. Meyer, R.C.C. Perera, M.D. Rubin, Solid State Ionics, 165 (2003) 309-314.

[30] D. Lupu, R. Sarbu, A. Biris, Int. J. Hydrogen Energy, 12 (1987) 425-426.

[31] D.A. Sheppard, T.D. Humphries, C.E. Buckley, Appl. Phys. A, 122 (2016) 406.

[32] D.A. Sheppard, M. Paskevicius, T.D. Humphries, M. Felderhoff, G. Capurso, J. Bellosta von Colbe, M. Dornheim, T. Klassen, P.A. Ward, J.A. Teprovich, C. Corgnale, R. Zidan, D.M. Grant, C.E. Buckley, Appl. Phys. A, 122 (2016) 395.

[33] R. Urbanczyk, M. Meggouh, R. Moury, K. Peinecke, S. Peil, M. Felderhoff, Appl. Phys. A, 122 (2016) 1-5.

[34] R.J. Westerwaal, M. Slaman, C.P. Broedersz, D.M. Borsa, B. Dam, R. Griessen, A. Borgschulte, W. Lohstroh, B. Kooi, G. ten Brink, K.G. Tschersich, H.P. Fleischhauer, J. Appl. Phys., 100 (2006) 063518-063518.

[35] K.M. Nicholson, D.S. Sholl, Inorg. Chem., 53 (2014) 11833-11848.

[36] H. Blomqvist, D. Noréus, J. Appl. Phys., 91 (2002) 5141-5148.

[37] S. Hayashi, Inorg. Chem., 41 (2002) 2238-2242.

[38] P. Zolliker, K. Yvon, J.D. Jorgensen, F.J. Rotella, Inorg. Chem., 25 (1986) 3590-3593.

[39] W.R. Myers, L.W.W. Wang, T.J. Richardson, M.D. Rubin, J. Appl. Phys., 91 (2002) 4879-4885.

[40] Y. Pivak, V. Palmisano, H. Schreuders, B. Dam, J. Mater. Chem. A, 1 (2013) 10972-10978.

[41] J. Zhang, Y.N. Huang, P. Peng, C. Mao, Y.M. Shao, D.W. Zhou, Int. J. Hydrogen Energy, 36 (2011) 5375-5382.

[42] J. Zhang, D.W. Zhou, L.P. He, P. Peng, J.S. Liu, J. Phys. Chem. Solids, 70 (2009) 32-39.

[43] U. Häussermann, H. Blomqvist, D. Noréus, Inorg. Chem., 41 (2002) 3684-3692.

[44] G.N. Garcia, J.P. Abriata, J.O. Sofo, G. García, Phys. Rev. B, 59 (1999) 11746-11754.

[45] T. Sato, H. Blomqvist, D. Noréus, J. Alloys Compd., 356 (2003) 494-496.

[46] Z. Gavra, M.H. Mintz, G. Kimmel, Z. Hadari, Inorg. Chem., 18 (1979) 3595-3597.

[47] D. Noréus, P.E. Werner, J. Less-Common Met., 97 (1984) 215-222.

[48] P. Lindberg, D. Noréus, M.R.A. Blomberg, P.E.M. Siegbahn, J. Chem. Phys., 85 (1986) 4530-4537.

[49] J. Genossar, P.S. Rudman, J. Phys. Chem. Solids, 42 (1981) 611-616.

[50] D. Noréus, P.E. Werner, Mater. Res. Bull., 16 (1981) 199-206.

[51] J.P. Darnaudery, M. Pezat, B. Darriet, P. Hagenmuller, Mater. Res. Bull., 16 (1981) 1237-1244.

[52] P. Zolliker, K. Yvon, Mater. Res. Bull., 21 (1986) 415-419.

[53] D. Noreus, L.G. Olsson, J. Chem. Phys., 78 (1983) 2419-2427.

[54] P. Zolliker, K. Yvon, C. Baerlocher, J. Less-Common Met., 115 (1986) 65-78.

[55] D. Noréus, L. Kihlborg, J. Less-Common Met., 123 (1986) 233-239.

[56] M.L. Post, J.J. Murray, J. Less-Common Met., 134 (1987) 15-26.

[57] S.F. Parker, K.P.J. Williams, T. Smith, M. Bortz, B. Bertheville, K. Yvon, Phys. Chem. Chem. Phys., 4 (2002) 1732-1737.

[58] T.J. Richardson, J.L. Slack, R.D. Armitage, R. Kostecki, B. Farangis, M.D. Rubin, Appl. Phys. Lett., 78 (2001) 3047-3049.

[59] P. vanderSluis, M. Ouwerkerk, P.A. Duine, Appl. Phys. Lett., 70 (1997) 3356-3358.

[60] D.G. Nagengast, A.T.M. van Gogh, E.S. Kooij, B. Dam, R. Griessen, Appl. Phys. Lett., 75 (1999) 2050-2052.

[61] Q. Zhao, Y. Li, Y. Song, X. Cui, D. Sun, F. Fang, Appl. Phys. Lett., 102 (2013) 161901.

[62] H. Zhang, X.L. Wang, Y.Q. Qiao, X.H. Xia, J.P. Tu, Appl. Surf. Sci., 257 (2011) 5759-5765.

[63] Y. Yamada, K. Tajima, M. Okada, M. Tazawa, A. Roos, K. Yoshimura, Thin Solid Films, 519 (2011) 2941-2945.

[64] S. Bao, Y. Yamada, K. Tajima, M. Okada, K. Yoshimura, Jpn J Appl Phys, 47 (2008) 7993-7997.

[65] Y. Suyun, O. Liuzhang, Z. Min, Rare Metals, 25 (2006) 295-299.

[66] B. Farangis, P. Nachimuthu, T.J. Richardson, J.L. Slack, R.C.C. Perera, E.M. Gullikson, D.W. Lindle, M. Rubin, Phys. Rev. B, 67 (2003) 085106.

[67] V. Parkhutik, E. Matveeva, Y. Makushok, E. Rayon, T.J. Richardson, J. Electrochem. Soc., 152 (2005) H209-H212.

[68] M. Rogers, S. Barcelo, X.B. Chen, T.J. Richardson, V. Berube, G. Chen, M.S. Dresselhaus, C.P. Grigoropoulos, S.S. Mao, Appl. Phys. A: Mater. Sci. Process., 96 (2009) 349-352.

[69] M. Orlova, J.-P. Rapin, K. Yvon, Inorg. Chem., 48 (2009) 5052-5054.

[70] B. Huang, K. Yvon, J. Alloys Compd., 178 (1992) 173-179.

[71] B. Huang, K. Yvon, P. Fischer, J. Alloys Compd., 204 (1994) 5-8.

[72] G. Renaudin, L. Guenee, K. Yvon, J. Alloys Compd., 350 (2003) 145-150.

[73] T.D. Humphries, D.A. Sheppard, C.E. Buckley, Chem. Commun., 51 (2015) 11248-11251.

[74] K. Yvon, G. Renaudin, C.M. Wei, M.Y. Chou, Phys. Rev. Lett., 94 (2005) 066403.

[75] J.F. Herbst, J. Alloys Compd., 337 (2002) 99-107.

[76] J.L. Jiang, S.L. Zhang, S.P. Huang, P. Wang, H.P. Tian, Comput. Mater. Sci., 74 (2013) 55-64.

[77] M. Di Chio, A. Ziggiotti, M. Baricco, Intermetallics, 16 (2008) 102-106.

[78] K. Miwa, T. Sato, M. Matsuo, K. Ikeda, T. Otomo, S. Deledda, B.C. Hauback, G. Li, S. Takagi, S.-i. Orimo, J. Phys. Chem. C, 120 (2016) 5926-5931.

[79] M. Kersting, R. Pöttgen, Z. Naturforsch. , 66 (2011) 651-653.

[80] L. Pei, S. Han, J. Wang, L. Hu, X. Zhao, B. Liu, Mat. Sci. Eng. B-Solid, 177 (2012) 1589-1595.

[81] A. Teresiak, M. Uhlemann, A. Gebert, J. Thomas, J. Eckert, L. Schultz, J. Alloys Compd., 481 (2009) 144-151.

[82] J.J. Didisheim, P. Zolliker, K. Yvon, P. Fischer, J. Schefer, M. Gubelmann, A.F. Williams, Inorg. Chem., 23 (1984) 1953-1957.

[83] M. Polanski, T. Plocinski, I. Kunce, J. Bystrzycki, Int. J. Hydrogen Energy, 35 (2010) 1257-1266.

[84] M. Polanski, K. Witek, T.K. Nielsen, L. Jaroszewicz, J. Bystrzycki, Int. J. Hydrogen Energy, 38 (2013) 2785-2789.

[85] J. Huot, S. Boily, E. Akiba, R. Schulz, J. Alloys Compd., 280 (1998) 306-309.

[86] S.S.S. Raman, D.J. Davidson, J.L. Bobet, O.N. Srivastava, J. Alloys Compd., 333 (2002) 282-290.

[87] R.A. Varin, S. Li, Z. Wronski, O. Morozova, T. Khomenko, J. Alloys Compd., 390 (2005) 282-296.

[88] M.D. Riktor, S. Deledda, M. Herrich, O. Gutfleisch, H. Fjellvåg, B.C. Hauback, Mat. Sci. Eng. B-Solid, 158 (2009) 19-25.

[89] Y. Wang, F. Cheng, C. Li, Z. Tao, J. Chen, J. Alloys Compd., 508 (2010) 554-558.

[90] A.-L. Chaudhary, S. Dietzel, H.-W. Li, E. Akiba, N. Bergemann, C. Pistidda, T. Klassen, M. Dornheim, Int. J. Hydrogen Energy.

[91] I.G. Konstanchuk, E.Y. Ivanov, M. Pezat, B. Darriet, V.V. Boldyrev, P. Hagenmuller, J. Less-Common Met., 131 (1987) 181-189.

[92] B. Bogdanović, A. Reiser, K. Schlichte, B. Spliethoff, B. Tesche, J. Alloys Compd., 345 (2002) 77-89.

[93] K. Miwa, S. Takagi, M. Matsuo, S.-i. Orimo, J. Phys. Chem. C, 117 (2013) 8014-8019.

[94] D.A. Sheppard, M. Paskevicius, C.E. Buckley, Chem. Mater., 23 (2011) 4298-4300.

[95] M. Polanski, T.K. Nielsen, Y. Cerenius, J. Bystrzycki, T.R. Jensen, Int. J. Hydrogen Energy, 35 (2010) 3578-3582.

[96] T.D. Humphries, M. Matsuo, G. Li, S.-i. Orimo, Phys. Chem. Chem. Phys., 17 (2015) 8276 - 8282.

[97] M. Paskevicius, D.A. Sheppard, C.E. Buckley, J. Am. Chem. Soc., 132 (2010) 5077-5083.

[98] X. Zhang, W. Tian, J. Yang, R. Yang, J. Zheng, X. Li, Mater. Trans., 52 (2011) 618-622.

[99] M. Polanski, J. Bystrzycki, R.A. Varin, T. Plocinski, Int. J. Hydrogen Energy, 36 (2011) 1059-1065.

[100] S.L. Li, R.A. Varin, T. Nonferr. Metal Soc., 14 (2004) 649-653.

[101] M. Danaie, A.A.C. Asselli, J. Huot, G.A. Botton, J. Phys. Chem. C, 116 (2012) 25701-25714.

[102] L. George, V. Drozd, A. Durygin, J. Chen, S.K. Saxena, Int. J. Hydrogen Energy, 34 (2009) 3410-3416.

[103] S.F. Parker, K.P.J. Williams, M. Bortz, K. Yvon, Inorg. Chem., 36 (1997) 5218-5221.

[104] H.L. Zhou, Y. Yu, H.F. Zhang, T. Gao, Eur. Phys. J. B, 79 (2011) 283-288.

[105] S.V. Halilov, D.J. Singh, M. Gupta, R. Gupta, Phys. Rev. B, 70 (2004) 195117.

[106] E. Orgaz, M. Gupta, J. Alloys Compd., 240 (1996) 107-115.

[107] R.D. Shannon, Acta Crystallogr A, 32 (1976) 751-767.

[108] B. Huang, K. Yvon, P. Fischer, J. Alloys Compd., 187 (1992) 227-232.

[109] K. Yvon, J.P. Rapin, N. Penin, Z. Ma, M.Y. Chou, J. Alloys Compd., 446–447 (2007) 34-38.

[110] S.F. Parker, J.W. Taylor, H. Herman, J.-P. Rapin, N. Penin, K. Yvon, J. Alloys Compd., 470 (2009) 80-84.

[111] M. Matsuo, H. Saitoh, A. Machida, R. Sato, S. Takagi, K. Miwa, T. Watanuki, Y. Katayama, K. Aoki, S.-i. Orimo, RSC Adv., 3 (2013) 1013-1016.

[112] H. Saitoh, S. Takagi, M. Matsuo, Y. Iijima, N. Endo, K. Aoki, S. Orimo, APL Mat., 2 (2014) 076103-076103.

[113] T. Ogata, T. Sato, S. Takagi, H. Saitoh, Y. Iijima, B. Paik, S.-i. Orimo, Mater. Trans., 58 (2017) 157-159.

[114] A. Reiser, B. Bogdanovic, K. Schlichte, Int. J. Hydrogen Energy, 25 (2000) 425-430.

[115] P. Zolliker, K. Yvon, P. Fischer, J. Schefer, Inorg. Chem., 24 (1985) 4177-4180.

[116] E.J. Ivanov, I. Konstanchuk, A. Stepanov, Y. Jie, M. Pezat, B. Darriet, Inorg. Chem., 28 (1989) 613-615.

[117] M. Norek, T.K. Nielsen, M. Polanski, I. Kunce, T. Plocinski, L.R. Jaroszewicz, Y. Cerenius, T.R. Jensen, J. Bystrzycki, Int. J. Hydrogen Energy, 36 (2011) 10760-10770.
[118] S. Deledda, B.C. Hauback, Nanotechnology, 20 (2009).
[119] S.F. Parker, S. Deledda, J. Phys. Chem. C, 116 (2012) 25206-25212.
[120] M.G. Shelyapina, V.M. Pinyugzhanin, N.E. Skryabina, B.C. Hauback, Phys. Solid State, 55 (2013) 12-20.
[121] H. Fahlquist, K. Kadir, D. Noréus, J. Alloys Compd., 579 (2013) 31-33.
[122] P. Selvam, K. Yvon, Int. J. Hydrogen Energy, 16 (1991) 615-617.
[123] J. Huot, H. Hayakawa, E. Akiba, J. Alloys Compd., 248 (1997) 164-167.
[124] R. Lindsay, R.O. Moyer, J.S. Thompson, D. Kuhn, Inorg. Chem., 15 (1976) 3050-3053.
[125] R.O. Moyer, R. Lindsay, D.F. Storey, Z. Phys. Chem. Neue Fol., 165 (1989) 83-94.
[126] R.O. Moyer Jr, S.M. Antao, B.H. Toby, F.G. Morin, D.F.R. Gilson, J. Alloys Compd., 460 (2008) 138-141.
[127] R.O. Moyer Jr, D.F.R. Gilson, B.H. Toby, J. Solid State Chem., 184 (2011) 1895-1898.
[128] F. Bonhomme, K. Yvon, P. Fischer, J. Alloys Compd., 186 (1992) 309-314.
[129] M.M. Barsan, R.O. Moyer Jr, I.S. Butler, D.F.R. Gilson, J. Alloys Compd., 424 (2006) 73-77.
[130] R.O. Moyer, J.R. Wilkins, P. Ryan, J. Alloys Compd., 290 (1999) 103-109.
[131] M.M. Barsan, I.S. Butler, D.F.R. Gilson, R.O. Moyer Jr, W. Zhou, H. Wu, T.J. Udovic, J. Phys. Chem. A, 116 (2012) 2490-2496.
[132] M.M. Barsan, I.S. Butler, D.F.R. Gilson, R.O. Moyer, Jr., W. Zhou, H. Wu, T.J. Udovic, J. Phys. Chem. A, 112 (2008) 6936-6938.
[133] H. Hagemann, R.O. Moyer, J. Alloys Compd., 330 (2002) 296-300.
[134] L.M. Lawson Daku, H. Hagemann, Phys. Rev. B, 76 (2007) 014118.
[135] D.F.R. Gilson, R.O. Moyer, Inorg. Chem., 51 (2012) 1231-1232.
[136] W. Grochala, P.P. Edwards, Chem. Rev., 104 (2004) 1283-1315.
[137] W.M. Mueller, J.P. Blackledge, G.G. Libowitz, Metal Hydrides, Academic Press, inc., 1968.
[138] B. Huang, K. Yvon, P. Fischer, J. Alloys Compd., 190 (1992) 65-68.

Table 1. Properties of [NiH$_4$]$^{4-}$ complexes including Average Electronegativity (X$_a$) of M atom (Allred-Rochow scale), Ni−H bond distances (of their deuterides), ΔH of decomposition of the complex hydride and ΔH of formation of binary metal hydride. M = Na, Mg, Sr, La, Yb, Ca.

	Space group	X_a	Lattice Parameter of deuteride (a, Å)	Average Ni−D bond distance (Å)	ΔH_{des} (kJ/mol H$_2$)	$\Delta H_f MH_2$ (kJ/mol H$_2$)
Na$_2$Mg$_2$NiH$_6$	$Pnma$	1.12	11.433(1) [69]	1.61(2) [69]	---	−113 [136]
SrMgNiH$_4$	$P2_1 3$	1.11	6.8953(4) [71]	1.614(8) [71]	---	−176 [71]
LaMg$_2$NiH$_7$	$P2_1/c$	1.18	13.9789(7) [72]	1.59(2) [72]	94 [77]	−209 [137]
YbMgNiH$_4$	$P2_1 3$	1.15	6.7114(6) [71]	1.608(7) [71]	111 [71]	−182 [75]
CaMgNiH$_4$	$P2_1 3$	1.14	6.7301(4) [70]	1.601(8) [70]	129 [70]	−174.5 [75]
Mg$_2$NiH$_4$	C_2/c	1.23	14.343 [38]	1.53(2) [38]	64.4 [13]	−74.5 [75]
EuMgNiH$_4$	$P2_1 3$	1.12	6.8486(7)* [71]	---	---	---
La$_2$MgNi$_2$H$_8$	$P 2_1/c$	1.08	11.84482(11) [19]	1.58∫ [19]	---	−209 [137]

* Lattice parameter of hydride; ∫ errors not provided.

Table 2. Structural properties of [FeH$_6$]$^{4-}$ complexes including Average Electronegativity (X_a) of M atom (Allred-Rochow scale) and Equatorial Fe−D bond distances. M = Na, Mg, Sr, Ba, Yb, Ca.

	Space group	Lattice Parameter of deuteride (a, Å)	Fe−D (Å)	X_A	ΔH (kJ/mol H$_2$)
Mg$_2$FeD$_6$	$Fm-3m$	6.430(1) [82]	1.556(5) [82]	1.23	77.4[92]
BaMg$_2$FeD$_8$	$P-3m1$	4.5683(4) [24]	1.577(3) [24]	1.14	--
SrMg$_2$FeD$_8$	$P-3m1$	4.5072(2) [108]	1.578(4) [108]	1.15	--
Yb$_4$Mg$_4$Fe$_3$D$_{22}$	$P4/mmm$	6.6839(5) [22]	1.586(5) [22]	1.14	137(3) [22]
Ca$_4$Mg$_4$Fe$_3$D$_{22}$	$P-43m$	6.7016(4) [138]	1.583(3) [138]	1.15	122(4) [22]
Na$_2$Mg$_2$FeD$_8$	$Pbam$	5.30527(8) [26]	1.592(6) [26]	1.12	94.5 [96]
Ca$_2$FeD$_6$	$Fm-3m$	7.040(2) [9]	1.618(5) [8]	1.04	153.7 [93]
Eu$_2$FeH$_6$	$Fm-3m$	7.23* [9]	1.648(5)* [9]	1.01	146.1 [93]
Sr$_2$FeH$_6$	$Fm-3m$	7.315* [9]	1.683(2)* [9]	0.99	--
EuMg$_2$FeH$_8$	$P-3m1$	4.5078(1)* [24]	--	1.16	--

* Lattice parameter of hydride

Table 3. Structural properties of [CoH$_5$]$^{4-}$ complexes including average electronegativity (X_a) of M atom (Allred-Rochow scale) and Equatorial Co−D bond distances. M = Mg, Sr, Yb, Ca.

	Space group	Lattice Parameter of deuteride (a, Å)	Co−D (Å)	X_A
Mg$_2$CoD$_5$	$P4/nmm$	4.463(4) [115]	1.515(3) [115]	1.23
Yb$_4$Mg$_4$Co$_3$D$_{19}$	$P-43m$	6.6809(2) [25]	1.546(5) [121]	1.145
Ca$_4$Mg$_4$Co$_3$D$_{19}$	$P-43m$	6.6591(1) [25]	1.546(3) [121]	1.135
Sr$_4$Mg$_4$Co$_3$D$_{19}$	$P-43m$	6.91372(8) [121]	1.552(2) [121]	1.11

Table 4. Structural properties of $[RuH_6]^{4-}$ complexes including Average Electronegativity (X_a) of M atom (Allred-Rochow scale), equatorial Ru−D bond distances, IR vibrational Ru−H stretching modes. M = Na, Mg, Sr, Ba, Yb, Ca, Li.

	Space group	Lattice Parameter of deuteride (a, Å)	Ru−D (Å)	X_A	v(Ru−H) (cm⁻¹)	ΔH (kJ/mol H₂)
Mg₂RuH₆	$Fm-3m$	6.6294(8) [9]	1.673(4) [9]	1.23	1783 [10]	---
BaMg₂RuH₈	$P42/mmc$	4.9623(1) [20]	1.717(2) [20]	1.14	---	---
Sr₂RuH₆	$Fm-3m$	7.6088(3)* [10]	1.69(1)* [10]	0.99	1482 [10]	---
Ca₂RuH₆	$Fm-3m$	7.222(3) [126]	1.700(2) [126]	1.04	1559 [10]	−175.0[a]
LiMg₂RuH₇	$P63/mmc$	4.6998(1) [23]	1.704(7) [23]	1.18	---	---
Li₄RuH₆	$R-3c$	8.1686(29) [11]	1.714(5) [11]	0.99	1527 [14]	---
Yb₂RuH₆	$Fm-3m$	7.2352(18) [127]	1.7223(19) [127]	1.06	1548 [127]	−185.9[a]
Ba₂RuH₆	$Fm-3m$	8.0166(7) [10]	1.73(1) [10]	0.97	1438 [10]	−154.7[a]
Na₂Mg₂RuH₈	$Pbam$	5.37969(5) [26]	1.749(2) [26]	1.12	---	125[b]
Na₄RuH₆	$R-3c$	9.1443(3) [11]	1.792(9) [11]	1.01	---	---

* Lattice parameter of hydride. [a] Ref [35]. [b] Ref [96].

Fig. 1. Ligand geometries of (a) tetrahedral $[NiH_4]^{4-}$ (b) square-pyramidal $[CoH_5]^{4-}$; and (c) octahedral $[TH_6]^{4-}$ (T = Fe, Ru) complexes.

Fig. 2. (a) Low Temperature Mg₂NiH₄ phase molecular geometry; (b) Low Temperature Mg₂NiH₄ phase unit cell; (c) High Temperature Mg₂NiH₄ phase molecular geometry; (d) High Temperature Mg₂NiH₄ phase unit cell. Red balls = Mg, green = Ni and beige = deuterium [38, 44].

Fig. 3. Bonding configurations in selected $[NiH_4]^{4-}$ complexes. (a) CaMgNiD₄; (b) Na₂Mg₂NiD₆ and (c) LaMg₂NiD₇. Red balls = Mg, green = Ni, beige = D, purple = Ca, yellow = Na and grey = La [69, 70, 72].

Fig. 4. Bonding configurations in (a) Mg₂FeD₆; (b) SrMg₂FeD₈, (c) Ca₄Mg₄Fe₃D₂₂ and unit cell representation of Ca₄Mg₄Fe₃D₂₂. Red balls = Mg, olive = Fe, beige = D, purple = Ca, teal = Sr [21, 82, 108].

Fig. 5. Molecular structures of $[CoD_5]^{4-}$ complexes. Unit cell (a) and $[CoD_5]^{4-}$ bonding geometry (b) of Mg₂CoD₅ and unit cell of Mg₆Co₂D₁₁ (c) [6, 17]. Red balls are Mg atoms, blue are Co atoms and beige are D atoms.

Fig. 6. Bonding configurations in (a) Mg₂RuD₆; (b) Na₄RuD₆; (c) BaMg₂RuD₈; and (d) LiMg₂RuD₇ [9, 11, 20, 23]. Red balls = Mg, maroon = Ru, beige = D, grey = Ba, light purple = Li, yellow = Na.
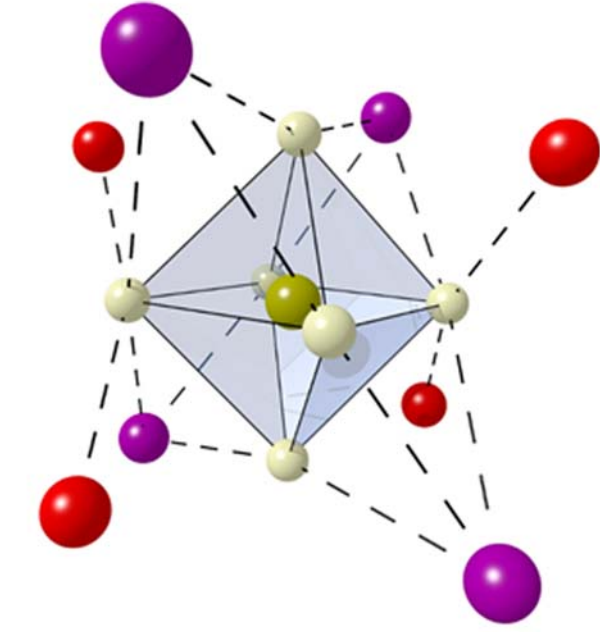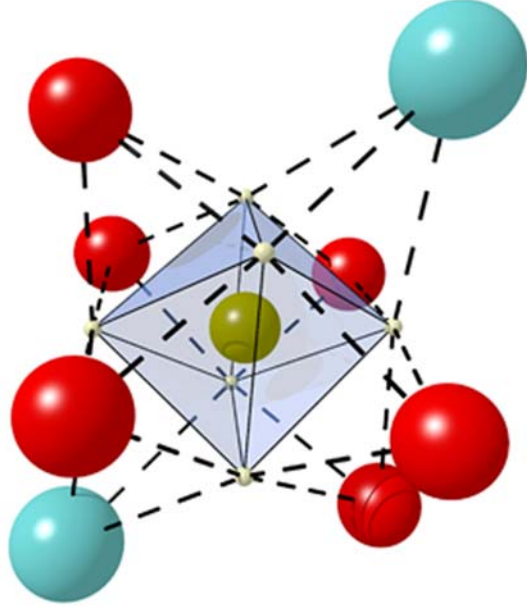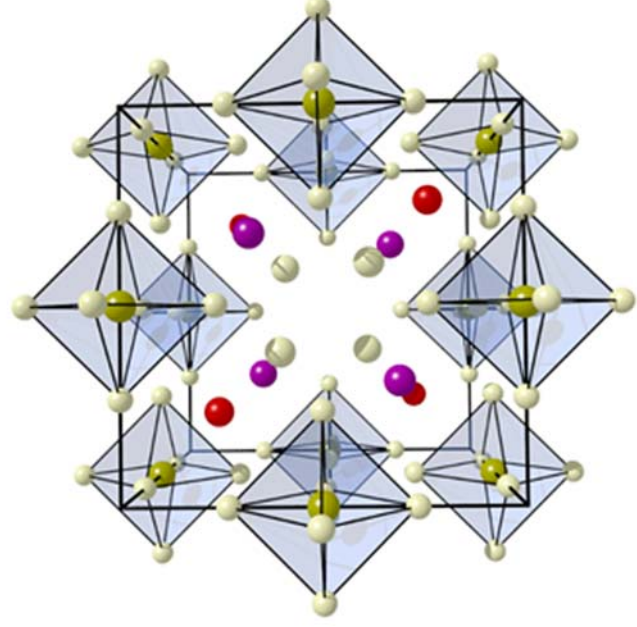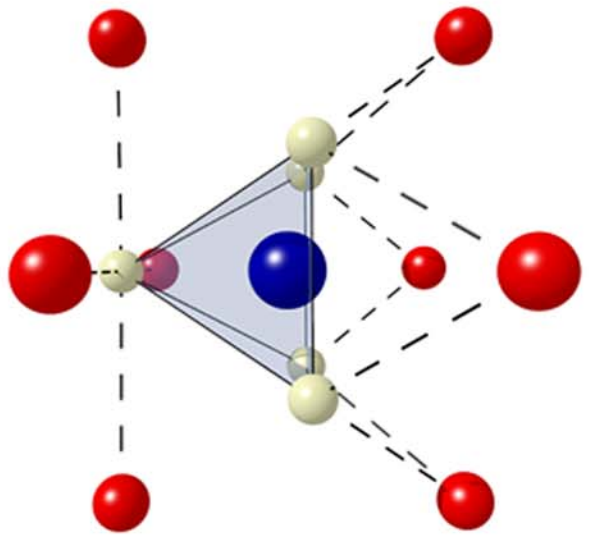
(a)

(b)

(c)

(a)

(b)

(c)

(d)

(a) (b) (c)
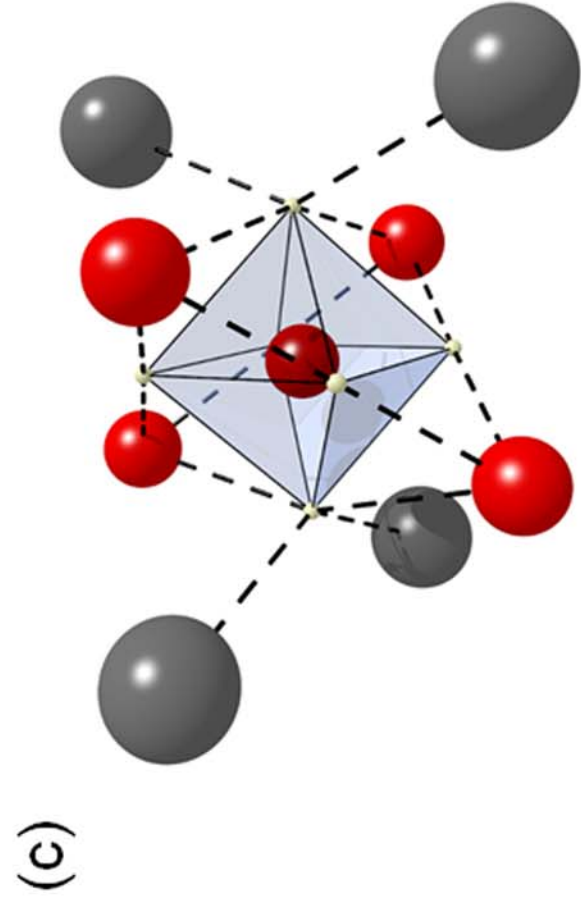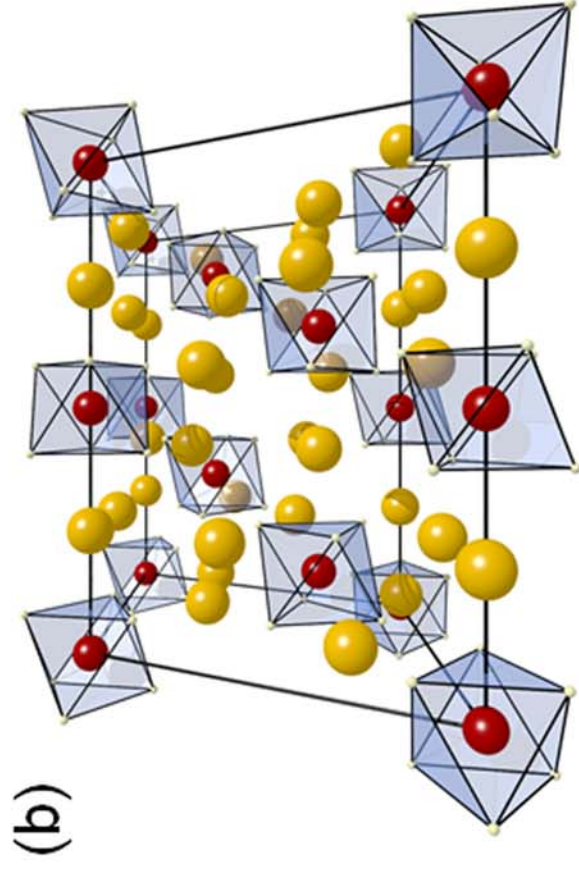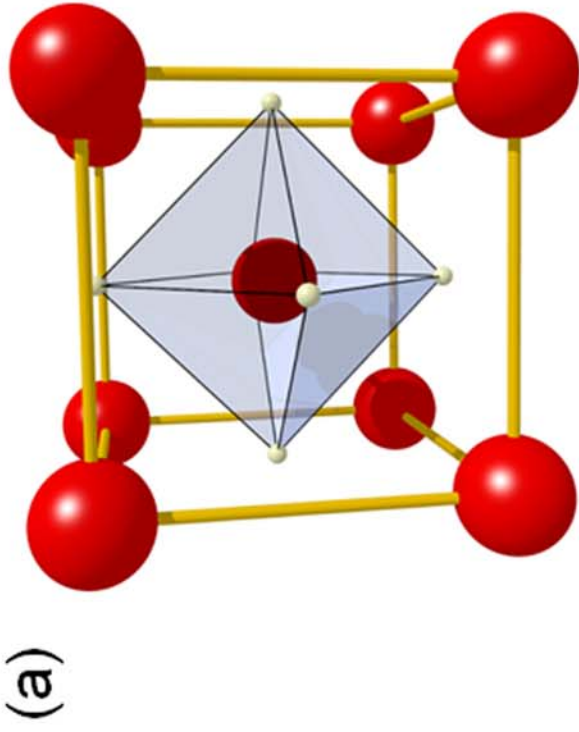
(a)

(b)

(c)

(d)

(a)

(b)

(c)

(a)

(b)
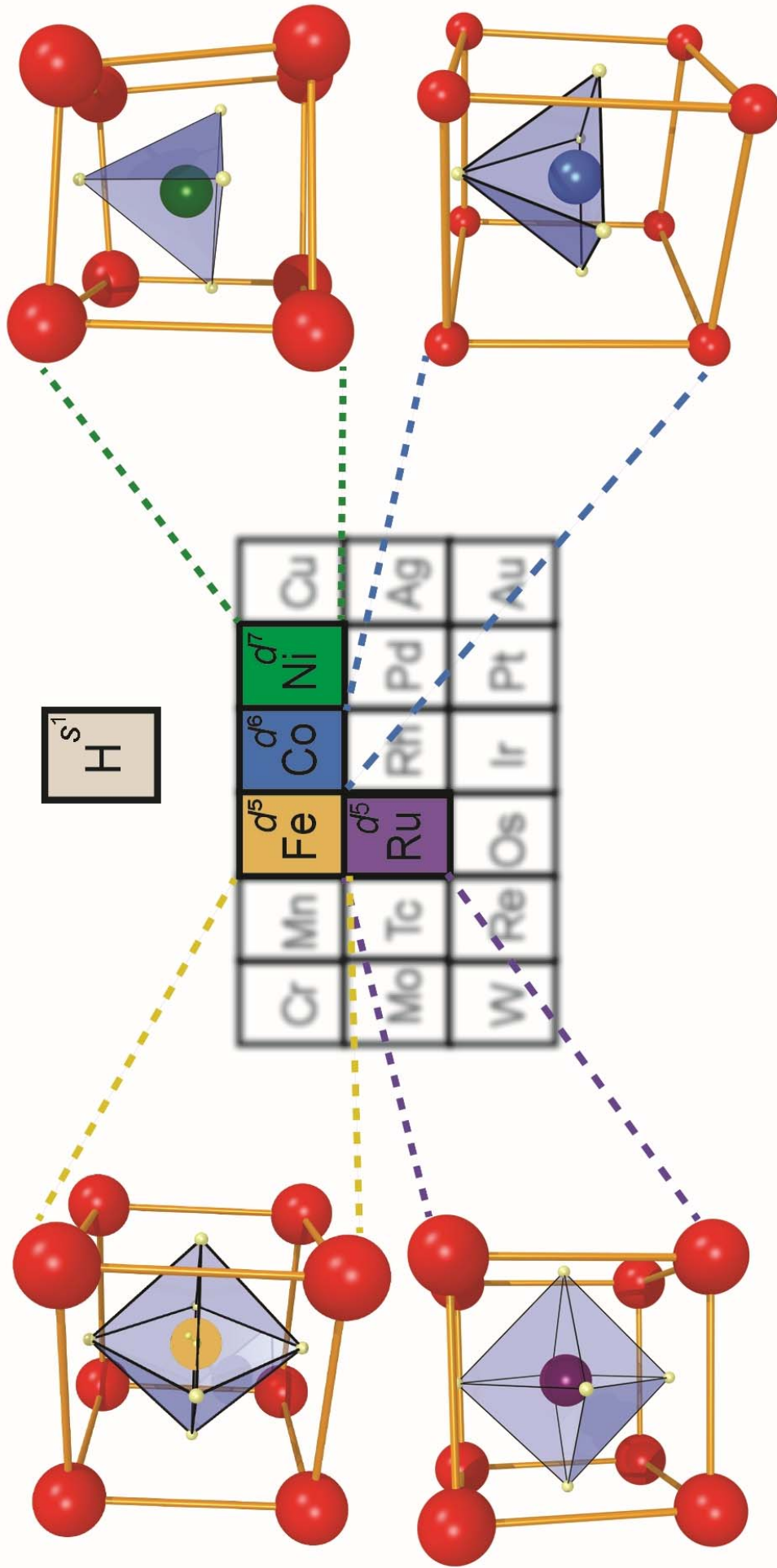
(c)

(d)
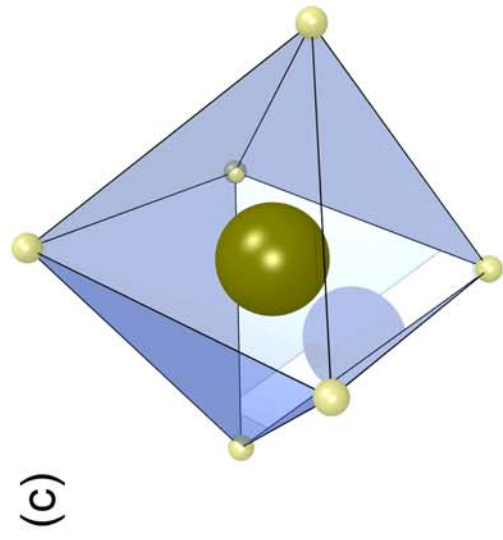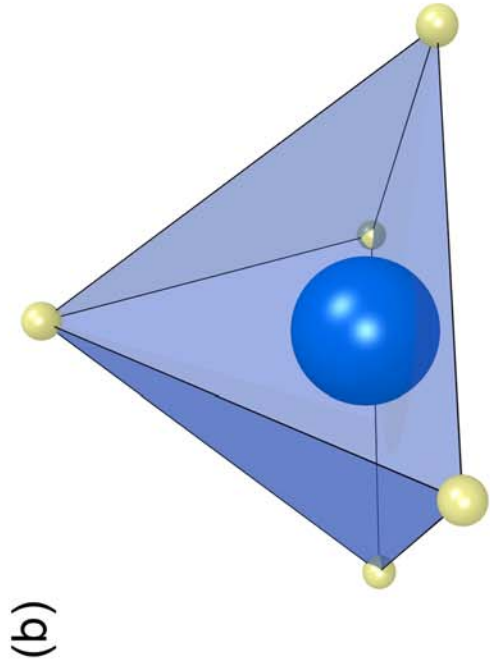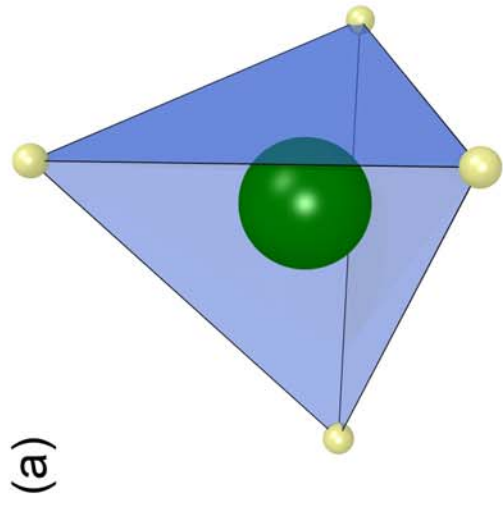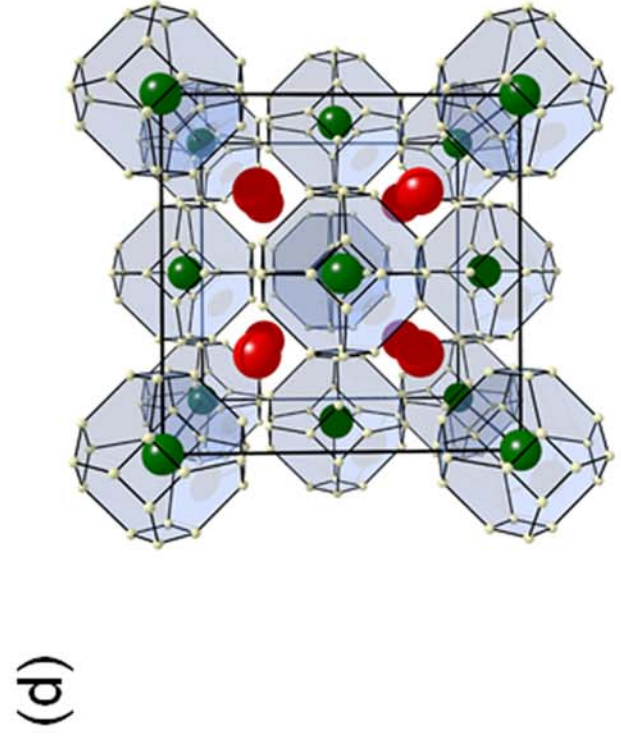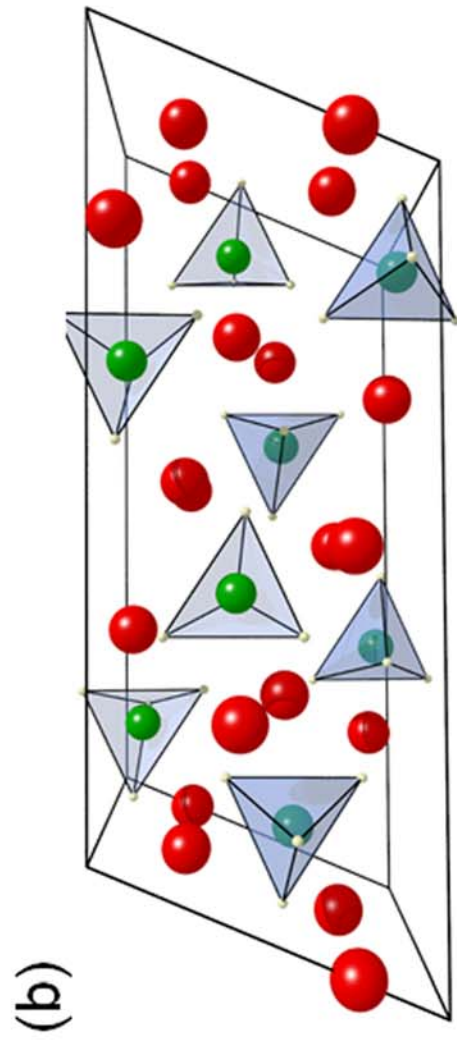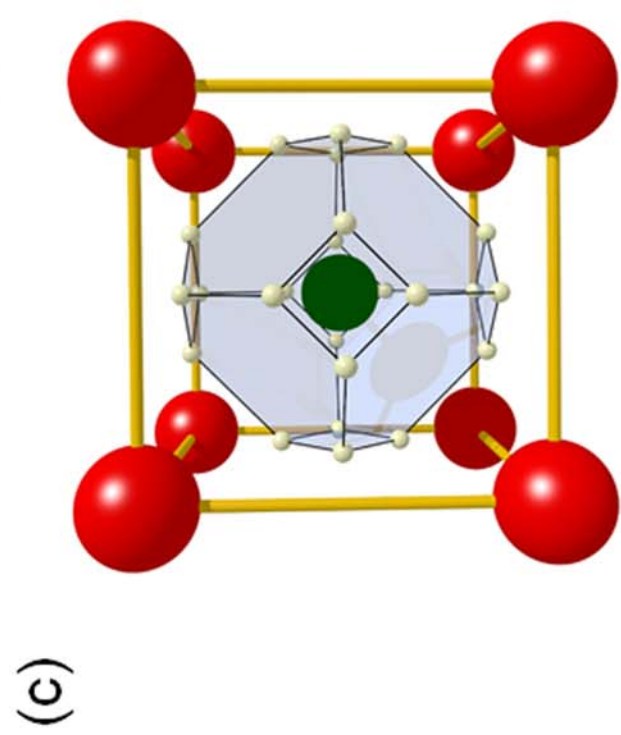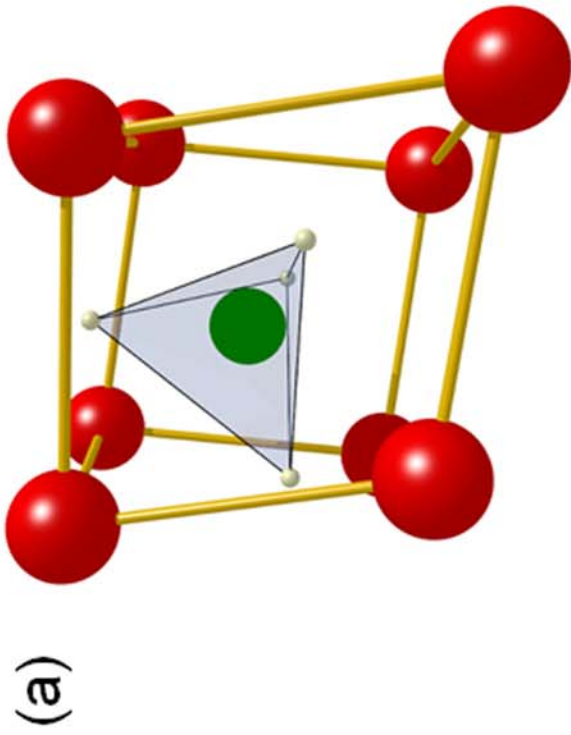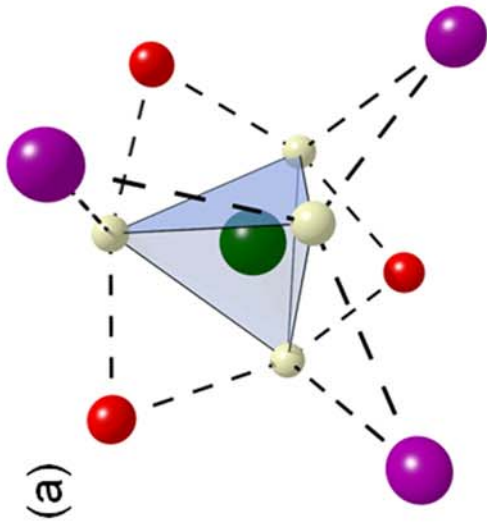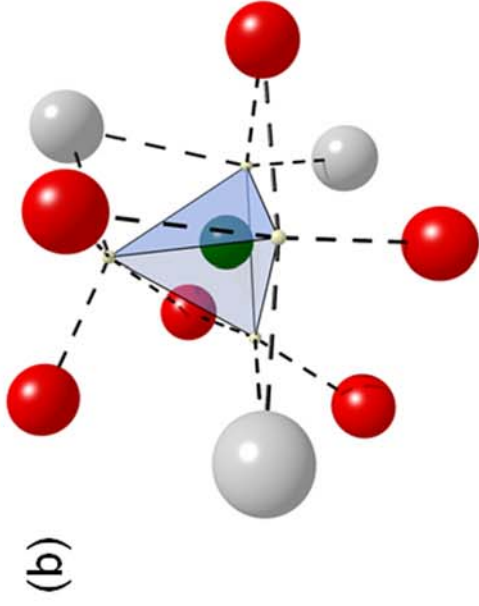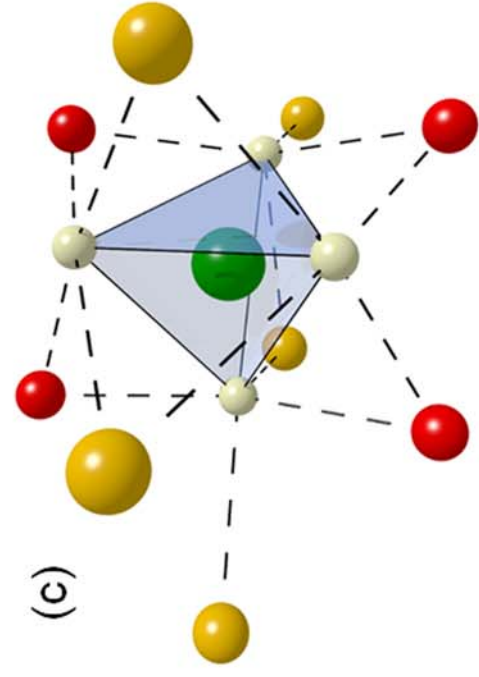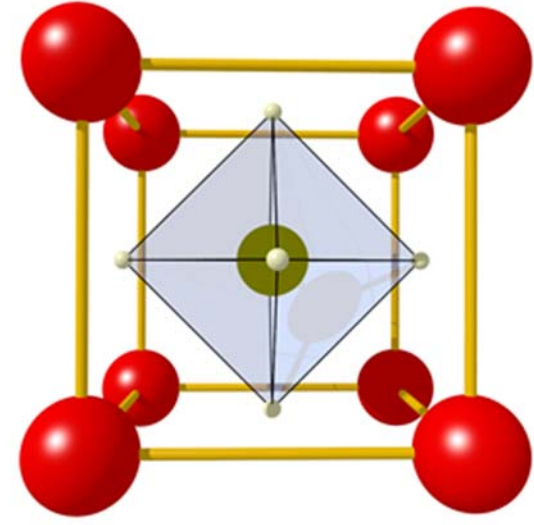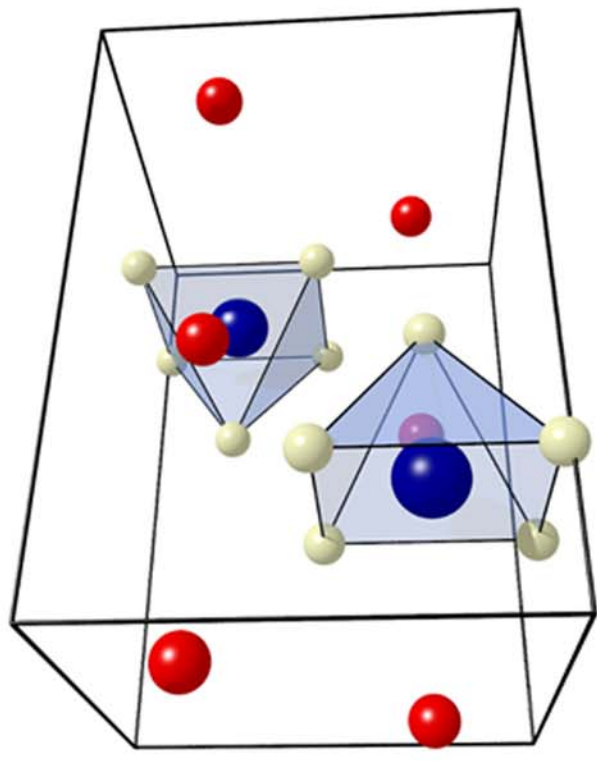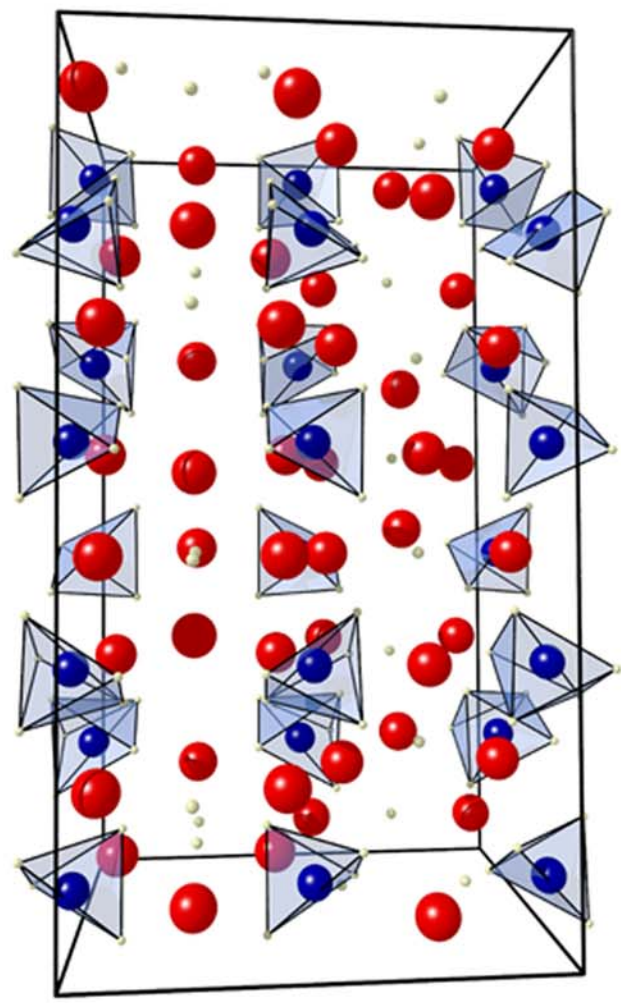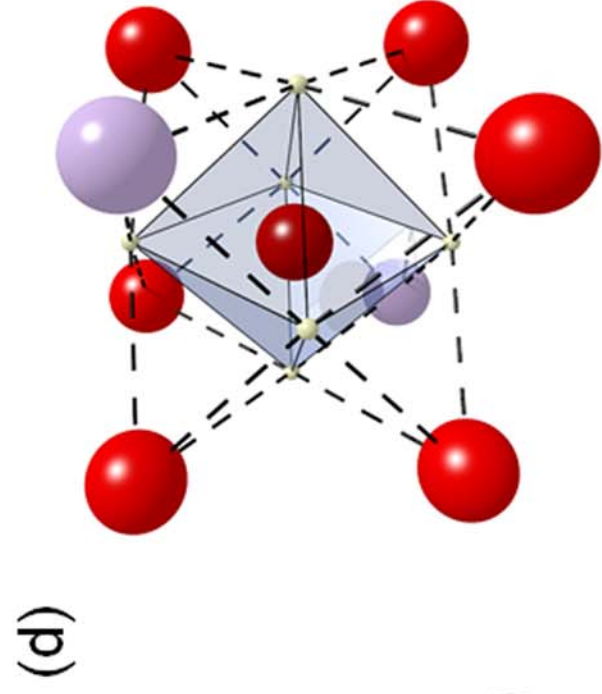
Highlights

- Complex Transition Metal Hydrides of Ni, Fe, Co and Ru have been explored.
- All analogues of $[NiH_4]^{4-}$, $[FeH_6]^{4-}$, $[CoH_5]^{4-}$ and $[RuH_6]^{4-}$ anions are detailed.
- Comprehensive description of molecular structures and physical properties of the complexes.
- These materials are determined to have multi-functional technological applications.